Formation and evolution of the Nuclear Star Cluster in the Milky Way and other spiral galaxies on the cosmological time scale.

CAMK, Polish Academy of Sciences, Warsaw, Poland.

MAO, National Academy of Sciences of Ukraine, Kiev.

JÜLICH Forschungszentrum | JÜLICH SUPERCOMPUTING CENTRE

VolkswagenStiftung

Dr. Sci. Peter Berczik

2024 August 19.

Formation and evolution of the Nuclear Star Cluster in the Milky Way and other spiral galaxies on the cosmological time scale.

PAN.BFB.S.BWZ.329.022.2023

Dr. Maryna Ishchenko
MAO, NASU
Warsaw / Kyiv

PhD student Margaryta Sobolenko
MAO, NASU
Warsaw / Kyiv

Dr. Oleksandr Veles
MAO, NASU
Kyiv / Warsaw

PhD student Olexander Sobodar
MAO, NASU
Kyiv / Warsaw

- **Peter Bertsyk**
- **Main Astronomical Observatory, National Academy of Sciences of Ukraine**
- **Nicolaus Copernicus Astronomical Centre of the Polish Academy of Sciences**

April 14, 2023

Milky Way globular clusters on cosmological timescales. I. Evolution of the orbital parameters in time-varying potentials

Maryna Ishchenko[1,2], Margaryta Sobolenko[1], Peter Berczik[3,4,1,2], Sergey Khoperskov[5,6], Chingis Omarov[2], Olexander Sobodar[1], and Maxim Makukov[2]

Milky Way globular clusters on cosmological timescales. II. Interaction with the Galactic centre

April 10, 2023

Maryna Ishchenko[1,2], Margaryta Sobolenko[1], Dana Kuvatova[2], Taras Panamarev[3,2], and Peter Berczik[4,5,2,1]

June 19, 2024

Dynamical evolution of Milky Way globular clusters on the cosmological timescale I. Mass loss and interaction with the nuclear star cluster

Maryna Ishchenko[1,2,3], Peter Berczik[2,3,8,1], Taras Panamarev[7,3], Dana Kuvatova[3], Mukhagali Kalambay[3,4,5,6], Anton Gluchshenko[3], Oleksandr Veles[1,2], Margaryta Sobolenko[1,2], Olexander Sobodar[1,2], and Chingis Omarov[3]

MAO, Kiev 8 node GPU cluster

MAO 4+4 new nodes 4xGF 2080S + 4xGF 3070 + 4xGF 4080

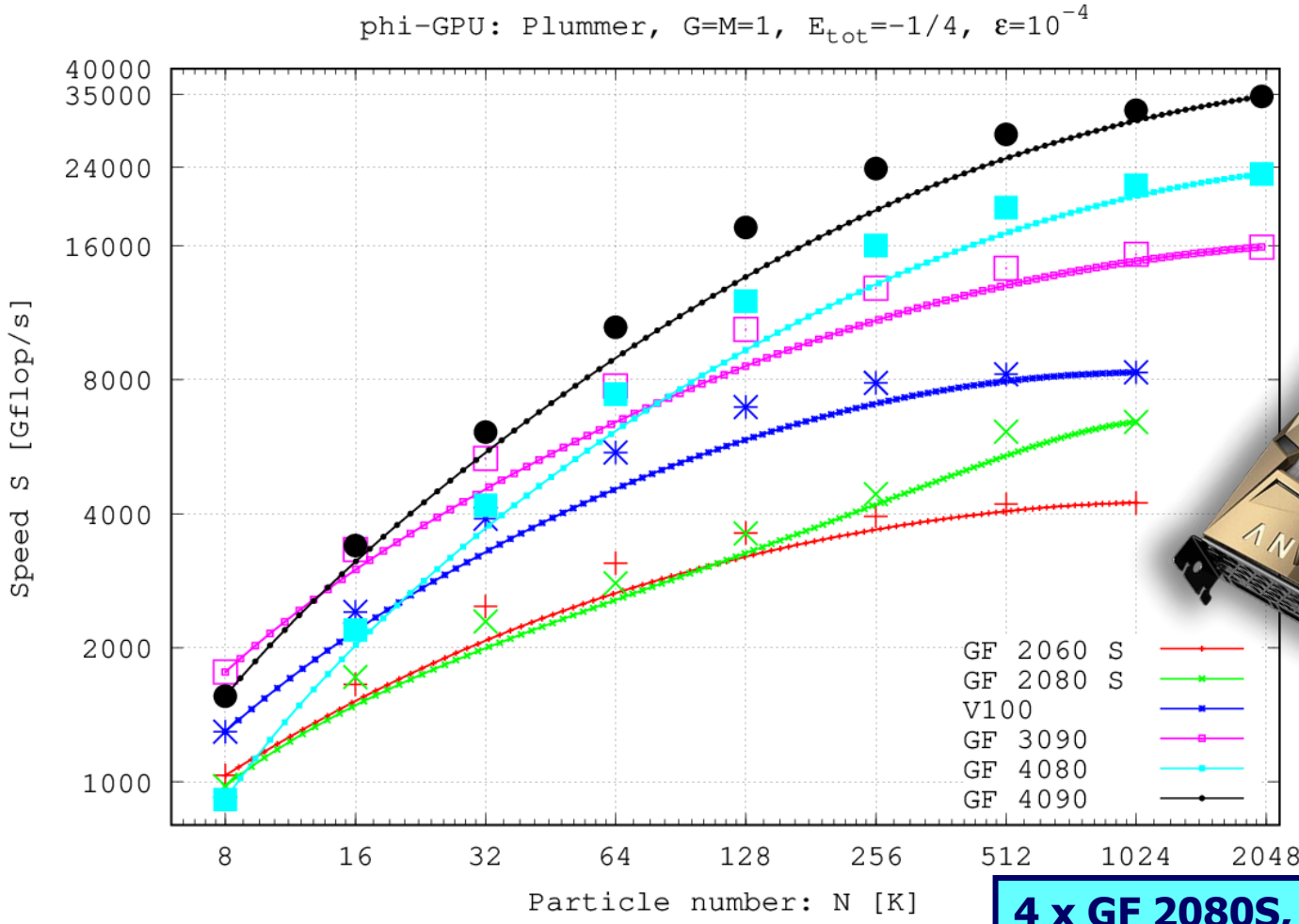

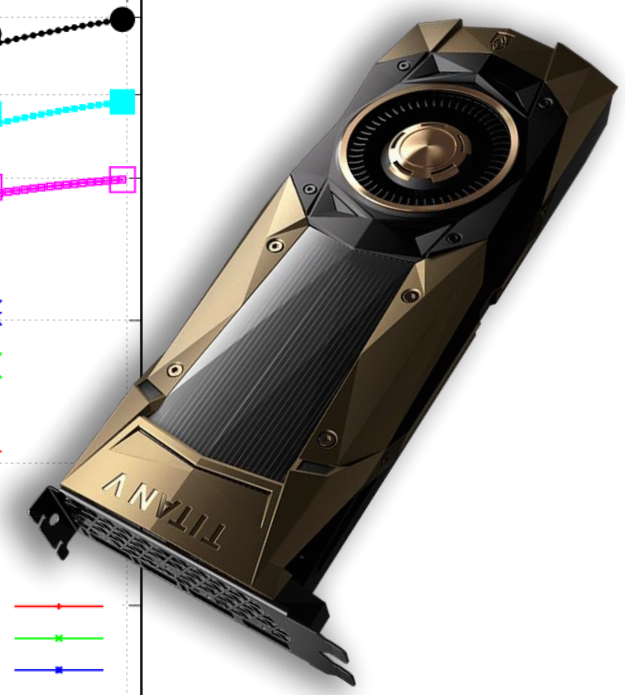

4 x GF 2080S, 3072 SP @ 1.81 GHz
4 x GF 3070, 5888 SP @ 1.77 GHz
4 x GF 4080, 9728 SP @ 2.54 GHz

Our φGPU (parallel) N-body code

Old GRAPE implementation: Harfst et al, NewA, 12, 357 (2007)

Hierarchical Individual Block Time Steps

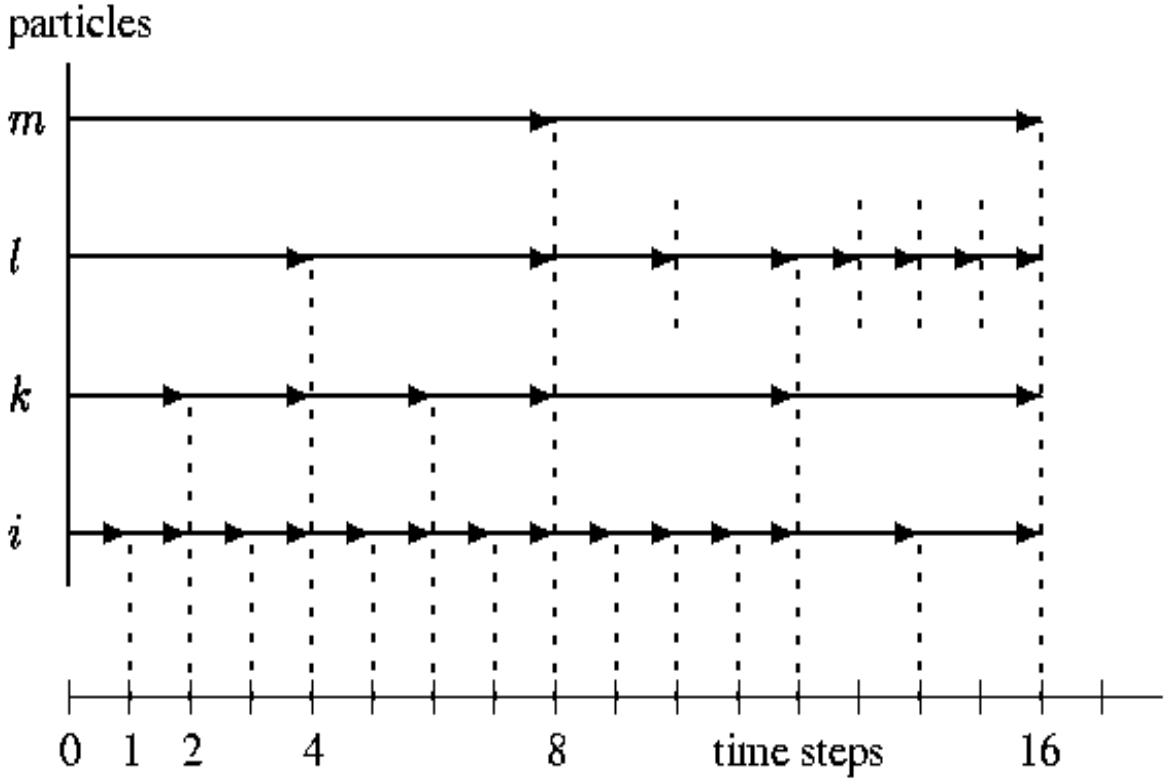

$$\Delta t = \sqrt{\eta \frac{|\vec{a}||\vec{a}^{(2)}| + |\dot{\vec{a}}|^2}{|\dot{\vec{a}}||\vec{a}^{(3)}| + |\vec{a}^{(2)}|^2}} \,.$$

4th order Hermite scheme

$$\frac{d^2\vec{r}_i}{dt^2} = \vec{a}_i$$

https://github.com/berczik/phi-GPU-mole

Our φGPU (parallel) N-body code

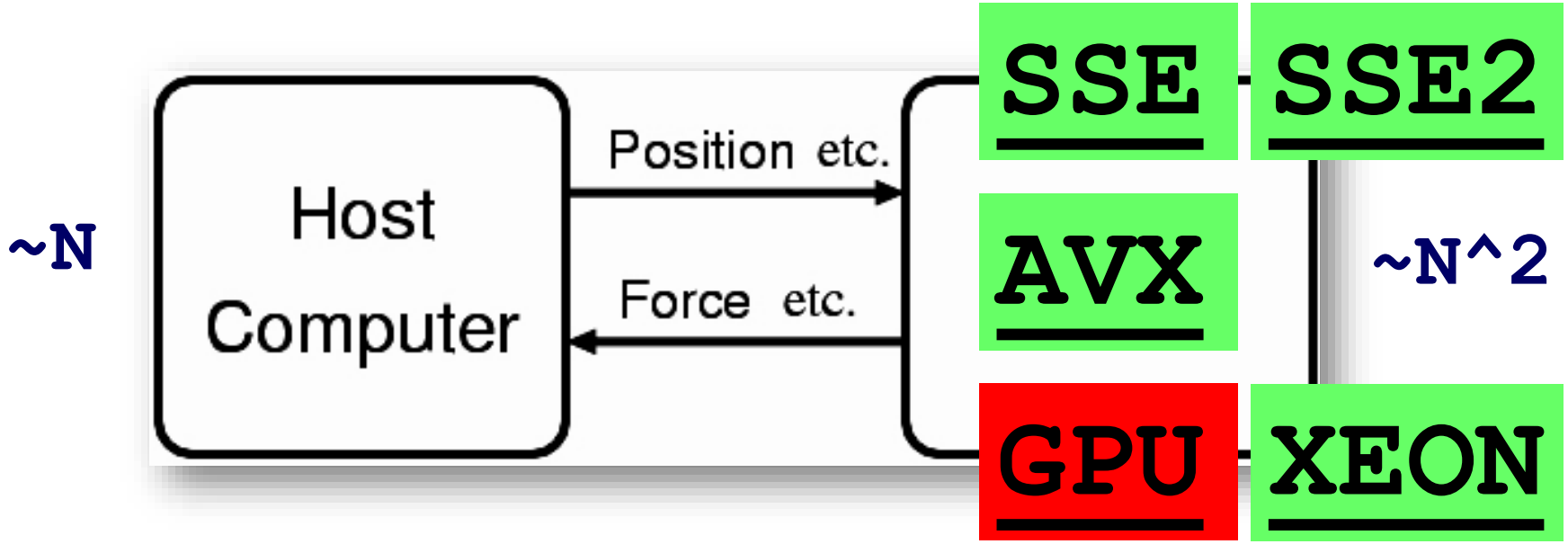

$$\vec{a}_i = \sum_{j=1;\, j\neq i}^{N} \vec{f}_{ij} \qquad \vec{f}_{ij} = -\frac{G \cdot m_j}{(r_{ij}^2 + \varepsilon^2)^{3/2}} \vec{r}_{ij}$$

https://github.com/berczik/phi-GPU-mole

Local Group and nearest galaxies

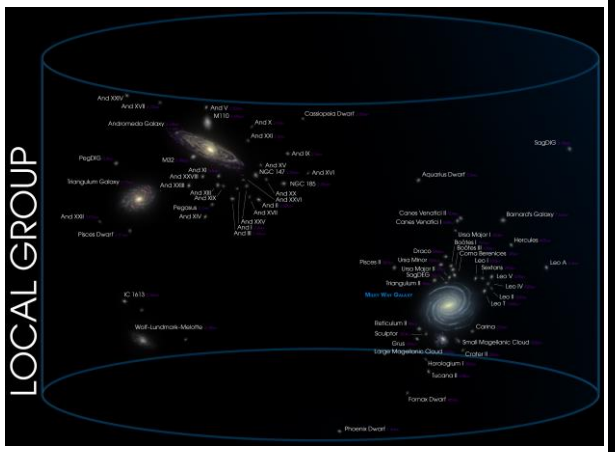

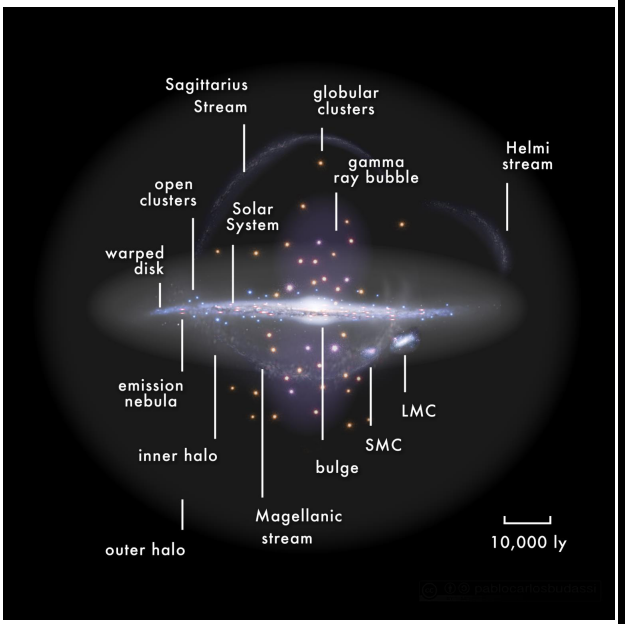

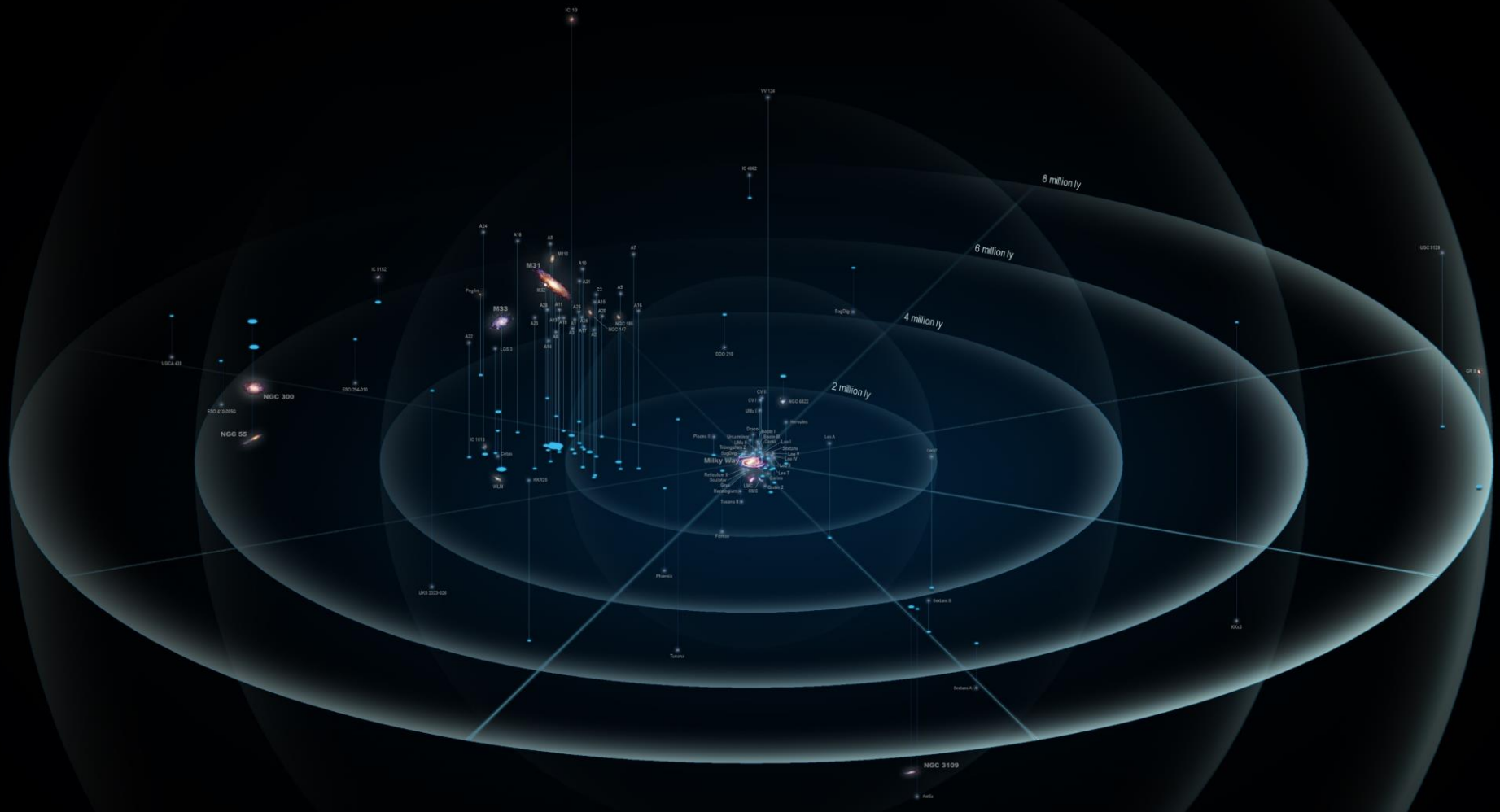

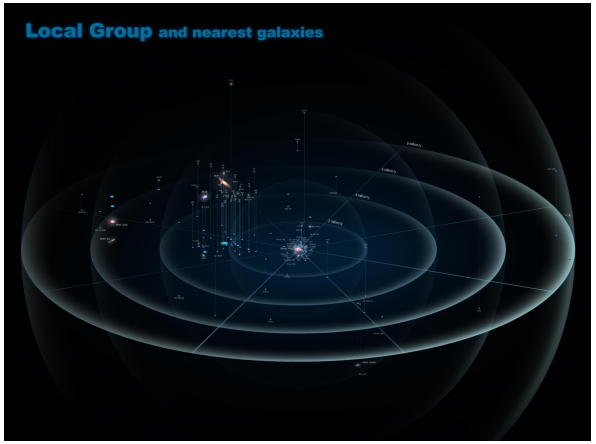

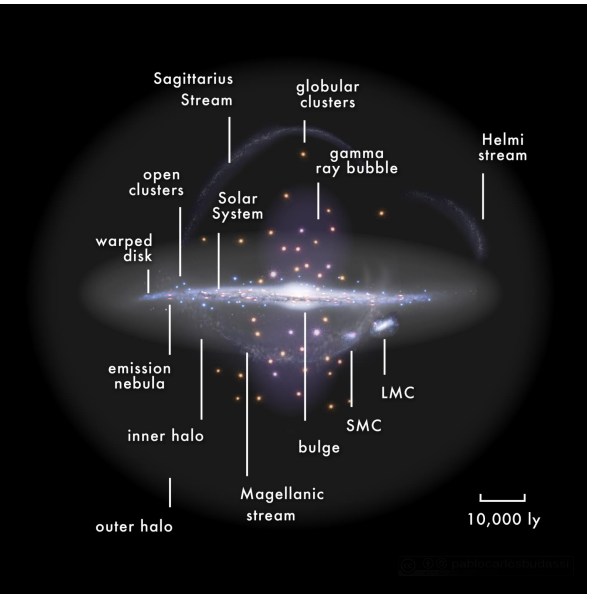

LOCAL GROUP

And XXIV
And XVII 4.42MLY
And V 2.52MLY
M110 2.69MLY
Cassiopeia Dwarf 2.58MLY
Andromeda Galaxy 2.54MLY
And X 2.9MLY
And XXI 2.8MLY
SagDIG 3.39MLY
PegDIG 3.0MLY
M32 2.49MLY
And IX 2.5MLY
And XV
NGC 147 2.53MLY
And XVI
And XI 2.6MLY
And XXVIII
Aquarius Dwarf 3.2MLY
Triangulum Galaxy 2.73MLY
And XXIII
NGC 185 2.05MLY
And XIII
And XIX
And XX
And XXVI
Pegasus 2.7MLY
And II 2.22MLY
And XVII
And XXII 3.07MLY
And XIV
And XXV
And I 2.4MLY
Canes Venatici II 506KLY
Barnard's Galaxy 1.63MLY
Canes Venatici I 698KLY
Pisces Dwarf 2.51MLY
And III 2.44MLY
Ursa Major I 330KLY
Hercules 455KLY
Boötes I 197KLY
Boötes III 150KLY
Draco 260KLY
Coma Berenices 140KLY
Pisces II 685KLY
Ursa Minor 200KLY
Leo I 820KLY
Leo A 2.6MLY
Ursa Major II 98KLY
Sextans 290KLY
SagDEG 65KLY
Leo V 678KLY
Triangulum II 98KLY
Leo IV 520KLY
IC 1613 2.38MLY
MILKY WAY GALAXY
Leo II 690KLY
Leo T 1365KLY
Reticulum II 98KLY
Carina 330KLY
Wolf–Lundmark–Melotte 3.04MLY
Sculptor 290KLY
Small Magellanic Cloud 200KLY
Grus 290KLY
Large Magellanic Cloud 163KLY
Crater II 383KLY
Horologium I 326KLY
Tucana II 228KLY
Fornax Dwarf 460KLY
Phoenix Dwarf 1.44MLY

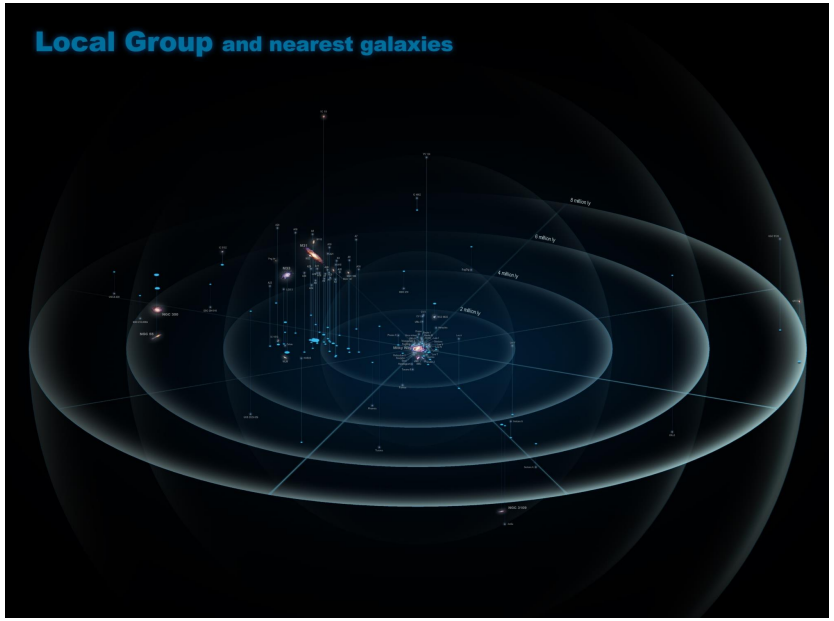
Local Group and nearest galaxies

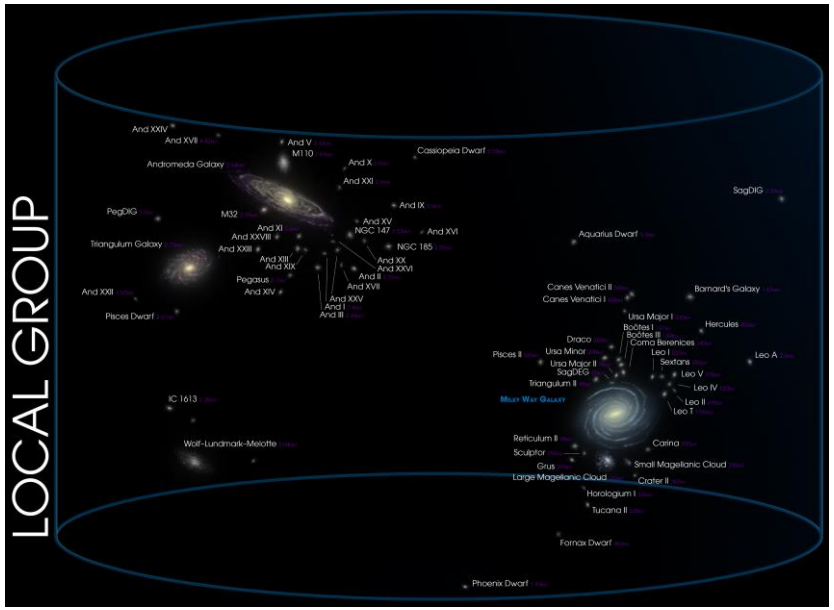
LOCAL GROUP
And XXIV
And XVII
And V
M110
Andromeda Galaxy
Cassiopeia Dwarf
And X
And XXI
SagDIG
And IX
PegDIG
M32
And XI
And XXVIII
Triangulum Galaxy
And XXIII
And XV
NGC 147
And XVI
NGC 185
Aquarius Dwarf
And XIII
And XIX
And XX
And XXVI
And II
And XVII
Pegasus
And XIV
And XXII
And XXV
And I
And III
Pisces Dwarf
Canes Venatici II
Canes Venatici I
Barnard's Galaxy
Ursa Major I
Hercules
Bootes I
Bootes III
Coma Berenices
Draco
Pisces II
Ursa Minor
Leo I
Leo A
Ursa Major II
Sextans
SagDEG
Leo V
Triangulum II
Leo IV
Milky Way Galaxy
Leo II
Leo T
IC 1613
Wolf-Lundmark-Melotte
Reticulum II
Carina
Sculptor
Small Magellanic Cloud
Grus
Large Magellanic Cloud
Crater II
Horologium I
Tucana II
Fornax Dwarf
Phoenix Dwarf

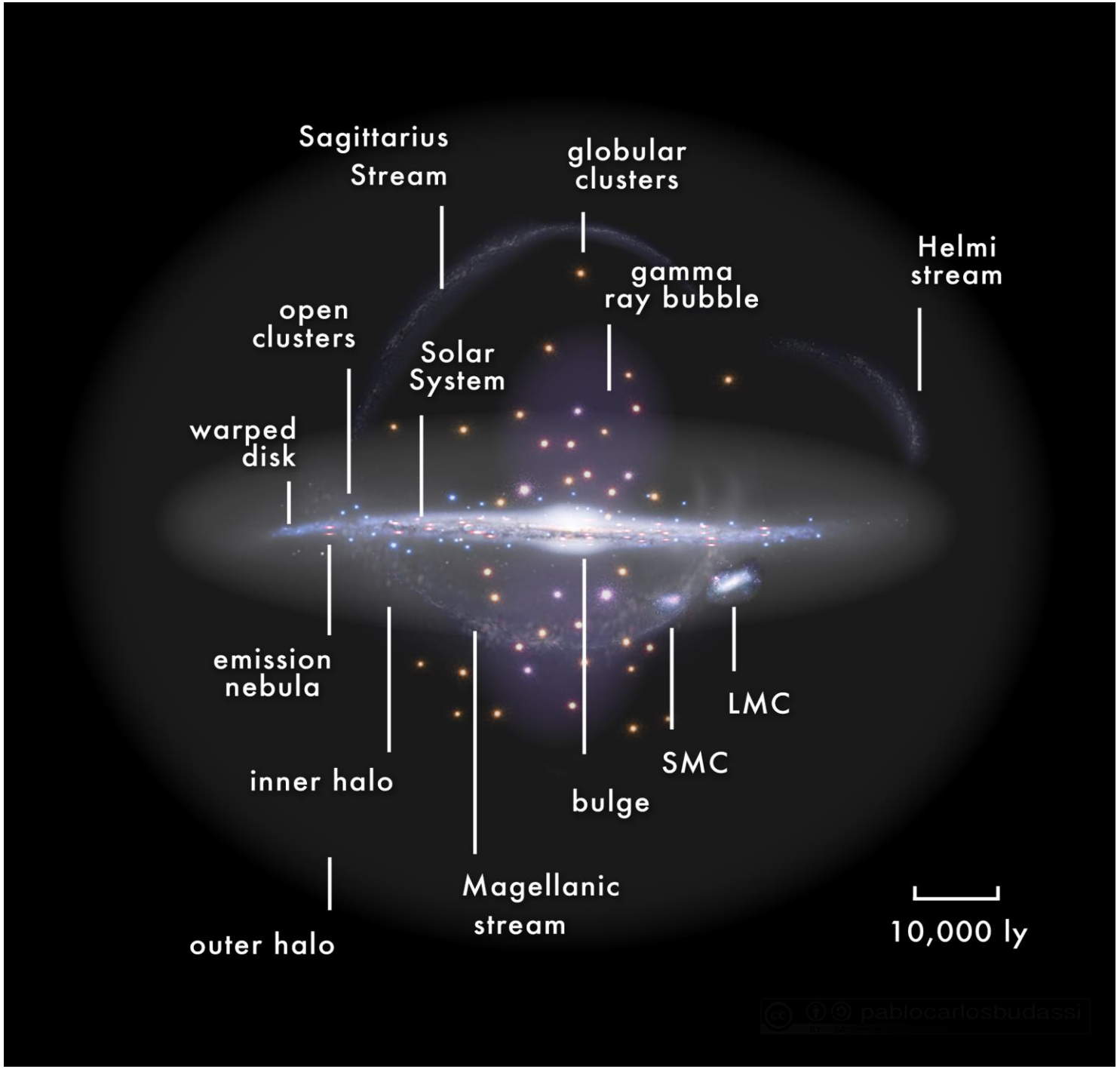
Sagittarius Stream
globular clusters
Helmi stream
gamma ray bubble
open clusters
Solar System
warped disk
emission nebula
inner halo
bulge
SMC
LMC
Magellanic stream
outer halo
10,000 ly
pablocarlosbudassi

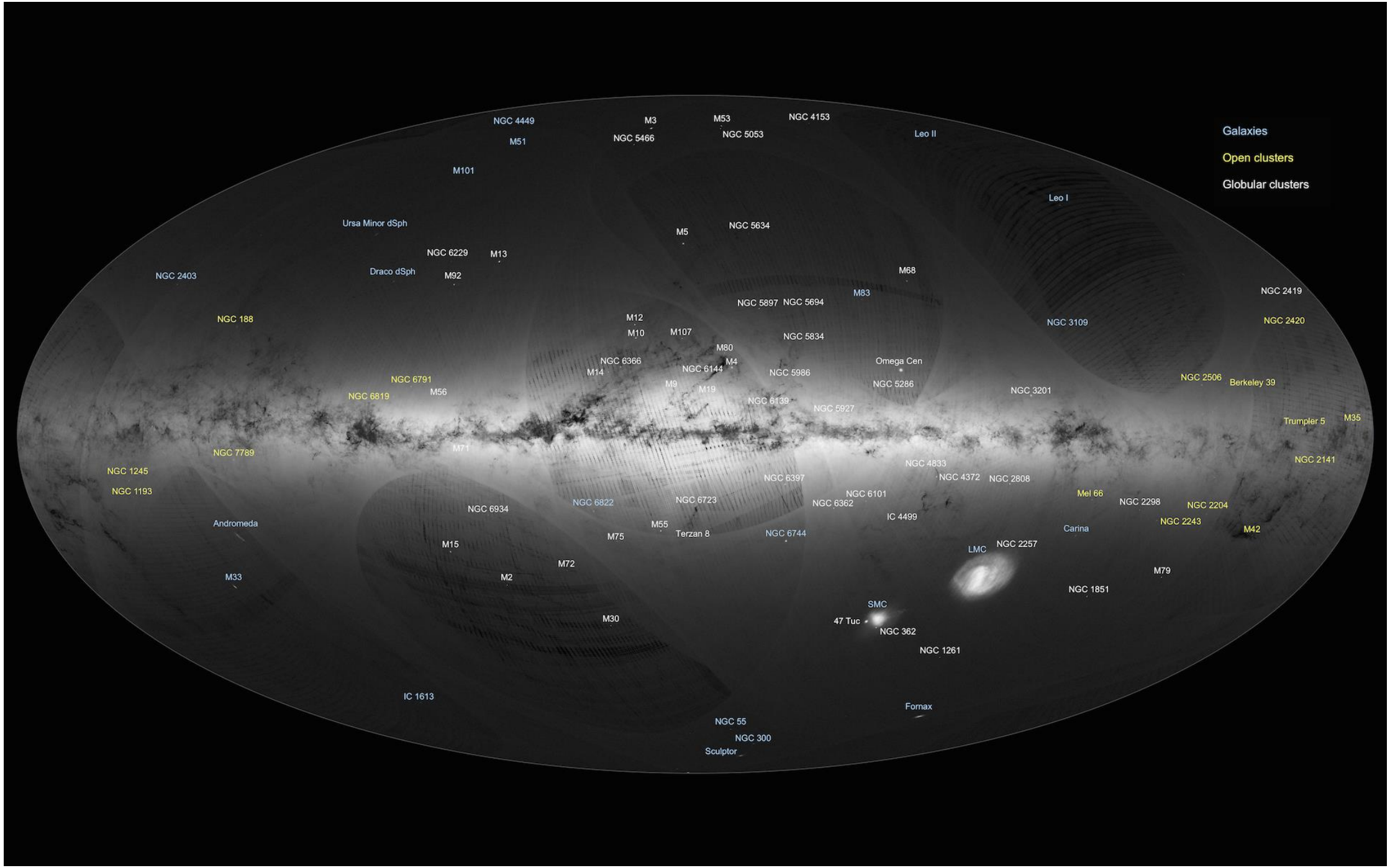
Galaxies
Open clusters
Globular clusters
NGC 4449
M3
M53
NGC 4153
M51
NGC 5466
NGC 5053
Leo II
M101
Leo I
Ursa Minor dSph
NGC 5634
M5
NGC 6229
M13
NGC 2403
Draco dSph
M92
M68
M83
NGC 2419
NGC 5897
NGC 5694
NGC 188
M12
NGC 3109
NGC 2420
M10
M107
NGC 5834
M80
NGC 6366
M4
Omega Cen
M14
NGC 6144
NGC 5986
NGC 6791
NGC 5286
NGC 2506
Berkeley 39
M9
M19
NGC 6819
M56
NGC 6139
NGC 3201
NGC 5927
Trumpler 5
M35
M71
NGC 7789
NGC 4833
NGC 2141
NGC 1245
NGC 6397
NGC 4372
NGC 2808
NGC 1193
NGC 6101
Mel 66
NGC 6822
NGC 6723
NGC 6362
NGC 2298
NGC 2204
NGC 6934
IC 4499
Andromeda
M55
NGC 2243
Carina
M42
M75
Terzan 8
NGC 6744
M15
LMC
NGC 2257
M72
M79
M33
M2
NGC 1851
SMC
M30
47 Tuc
NGC 362
NGC 1261
IC 1613
Fornax
NGC 55
NGC 300
Sculptor

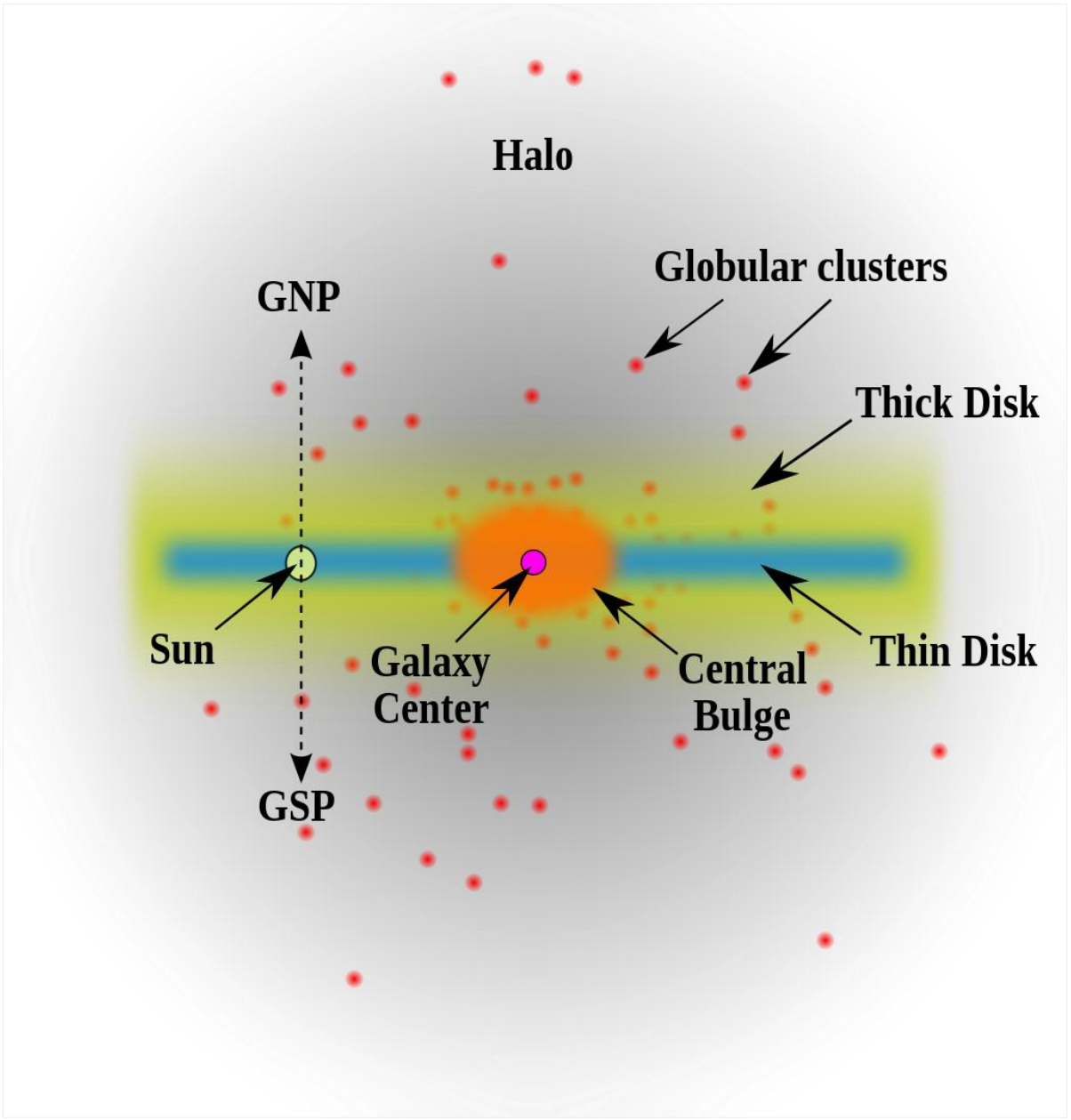
Halo
Globular clusters
GNP
Thick Disk
Sun
Galaxy Center
Central Bulge
Thin Disk
GSP

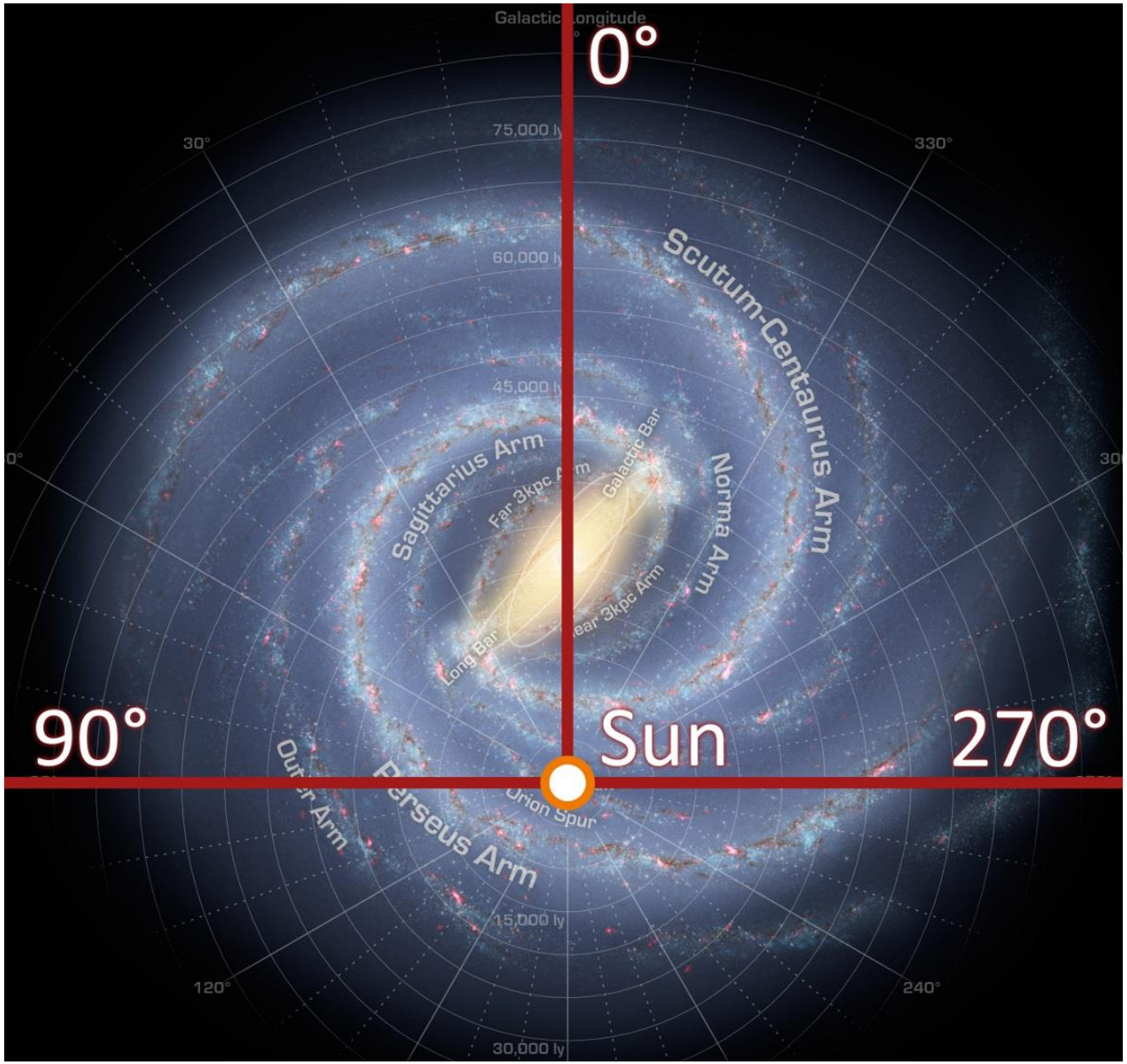
Galactic Longitude
0°
30°
330°
75,000 ly
60,000 ly
45,000 ly
Scutum-Centaurus Arm
Sagittarius Arm
Far 3kpc Arm
Galactic Bar
Norma Arm
Near 3kpc Arm
Long Bar
90°
Sun
270°
Outer Arm
Perseus Arm
Orion Spur
15,000 ly
120°
240°
30,000 ly

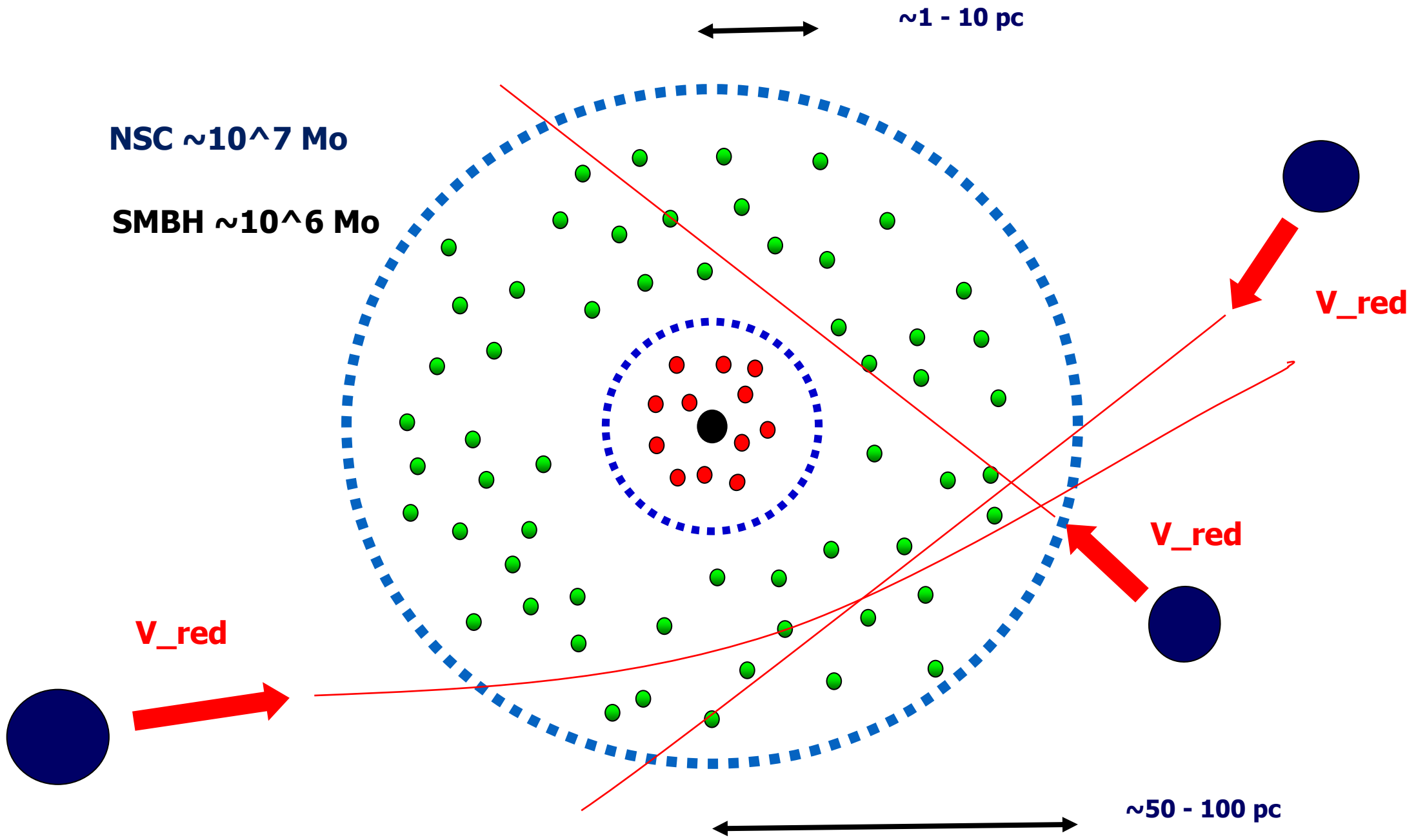
~1 - 10 pc
NSC ~10^7 Mo
SMBH ~10^6 Mo
V_red
V_red
V_red
~50 - 100 pc

https://www.tng-project.org

-The TNG Collaboration

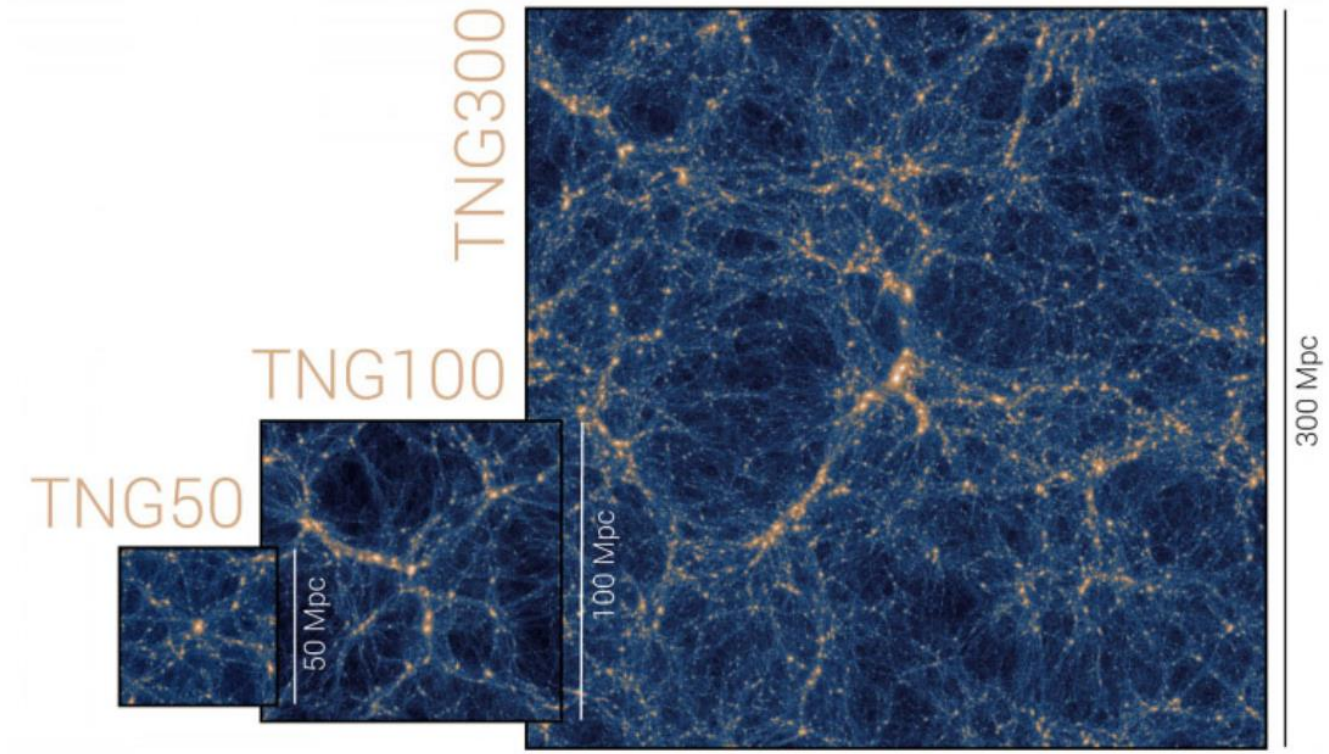

		TNG50	TNG100	TNG300
Volume	$[\mathrm{Mpc}^3]$	51.7^3	110.7^3	302.6^3
L_{box}	$[\mathrm{Mpc}/h]$	35	75	205
N_{GAS}	-	2160^3	1820^3	2500^3
N_{DM}	-	2160^3	1820^3	2500^3
N_{TR}	-	2160^3	2×1820^3	2500^3
m_{baryon}	$[\mathrm{M}_\odot]$	8.5×10^4	1.4×10^6	1.1×10^7
m_{DM}	$[\mathrm{M}_\odot]$	4.5×10^5	7.5×10^6	5.9×10^7
$\epsilon_{\mathrm{gas,min}}$	[pc]	74	185	370
$\epsilon_{\mathrm{DM},\star}$	[pc]	288	740	1480

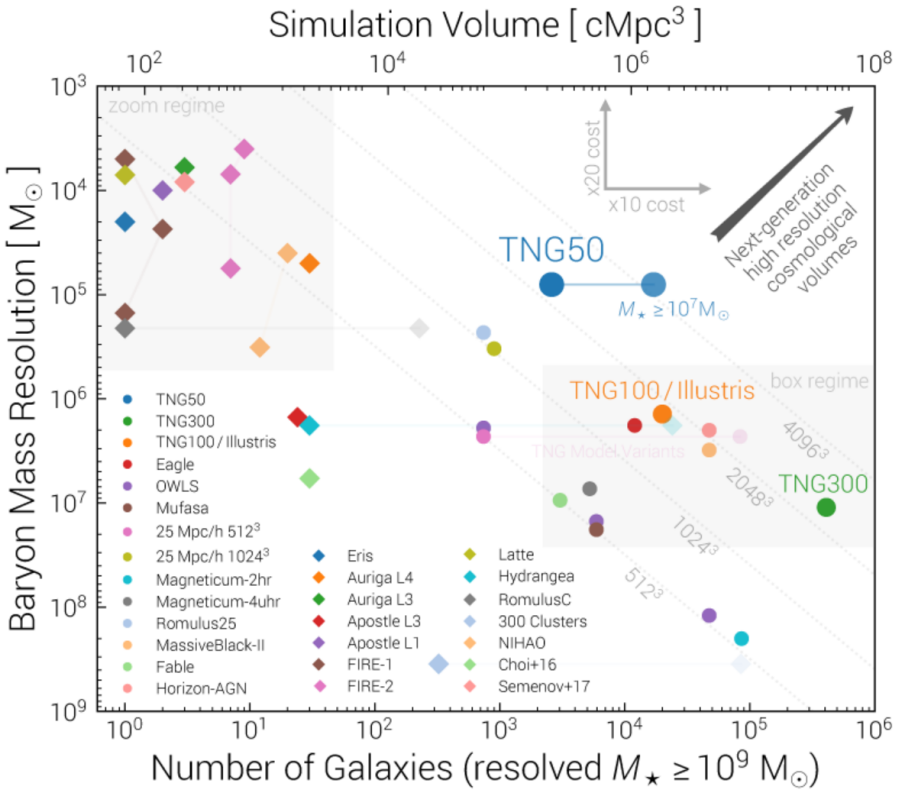

Volker Springel

Heidelberg Institute for Theoretical Studies ➔ MPA

PI: Overall TNG Project

Lars Hernquist

Harvard University

https://www.tng-project.org

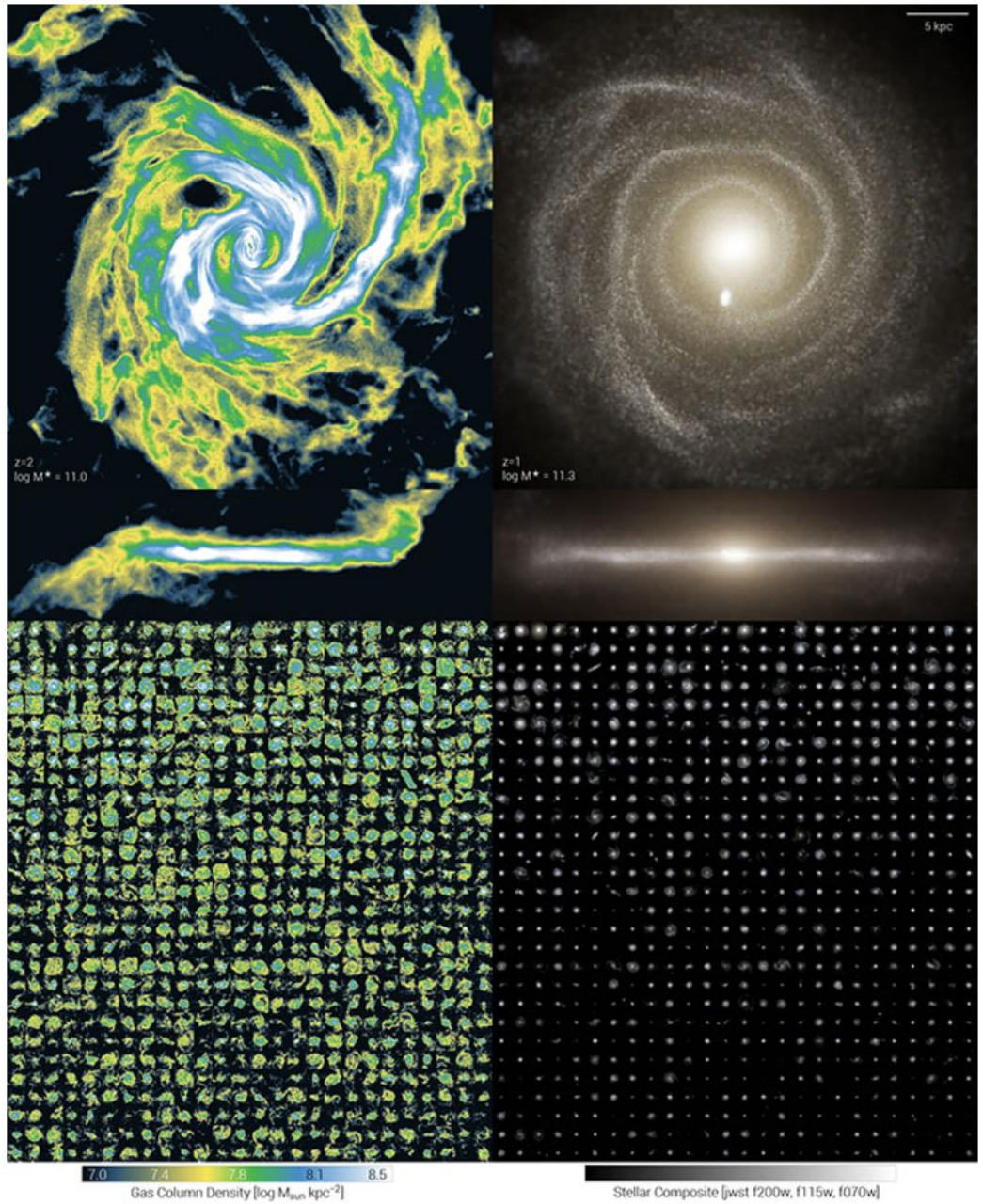

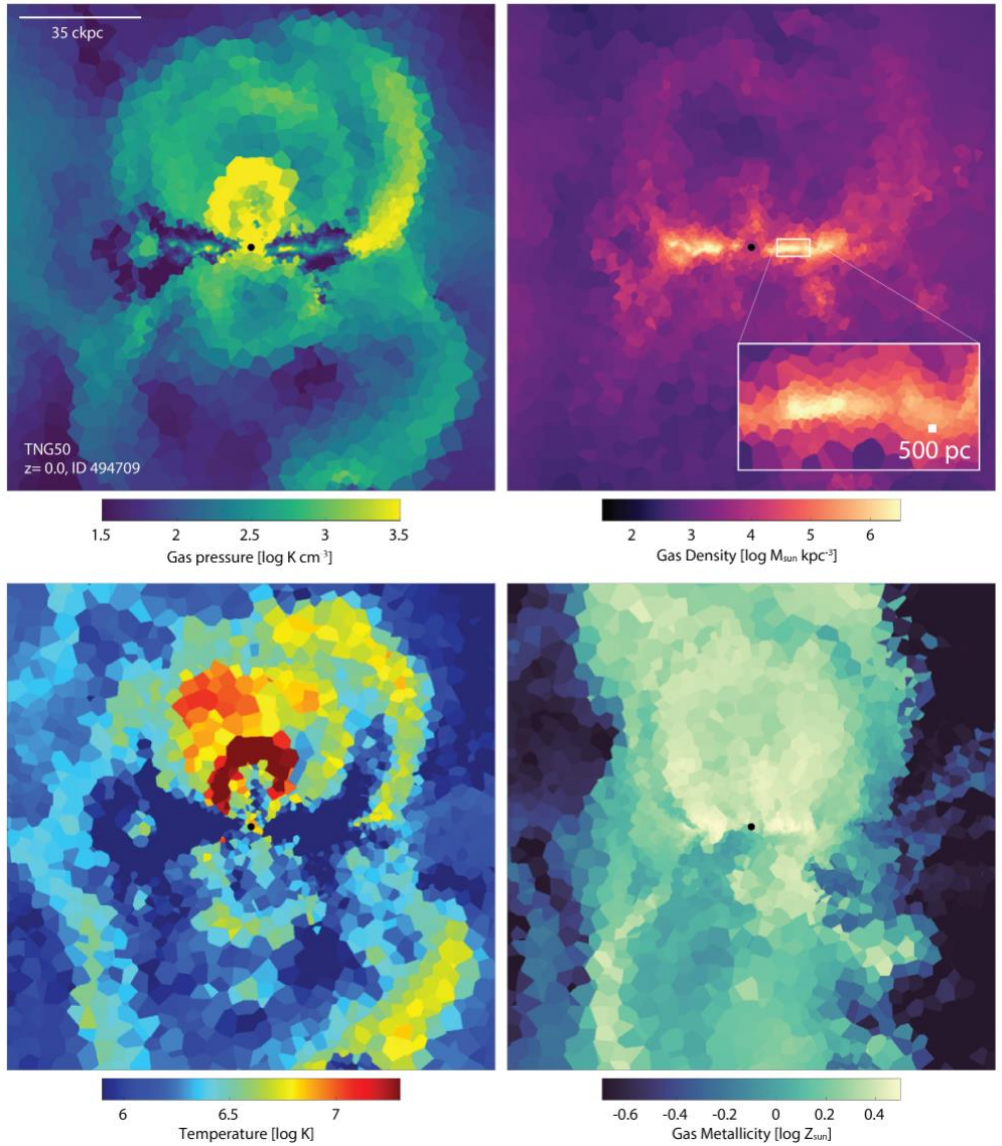

The gaseous (left) and stellar (right) structure of TNG50 galaxies at high redshift. The top shows a massive disk galaxy at z=2 and a descendant at z=1, while the bottom montage reveals ~750 central galaxies at redshift two, from large ellipticals at the center of galaxy groups to smaller, dwarf systems. [large] [ref]

A outflow-driven "bubble" produced by supermassive black hole feedback, around a disky galaxy similar to our own Milky Way at redshift zero, found within the TNG50 simulation. This structure is similar to those observed in gamma-rays by the Fermi telescope, and in x-rays by the eROSITA mission, in our own Galaxy. [large] [ref]

Milky Way and Andromeda analogs from the TNG50 simulation

Annalisa Pillepich[1,⋆], Diego Sotillo-Ramos[1], Rahul Ramesh[2], Dylan Nelson[2], Christoph Engler[1]
Vicente Rodriguez-Gomez[3], Martin Fournier[1], Martina Donnari[1], Volker Springel[4], and Lars Hernquist[5]

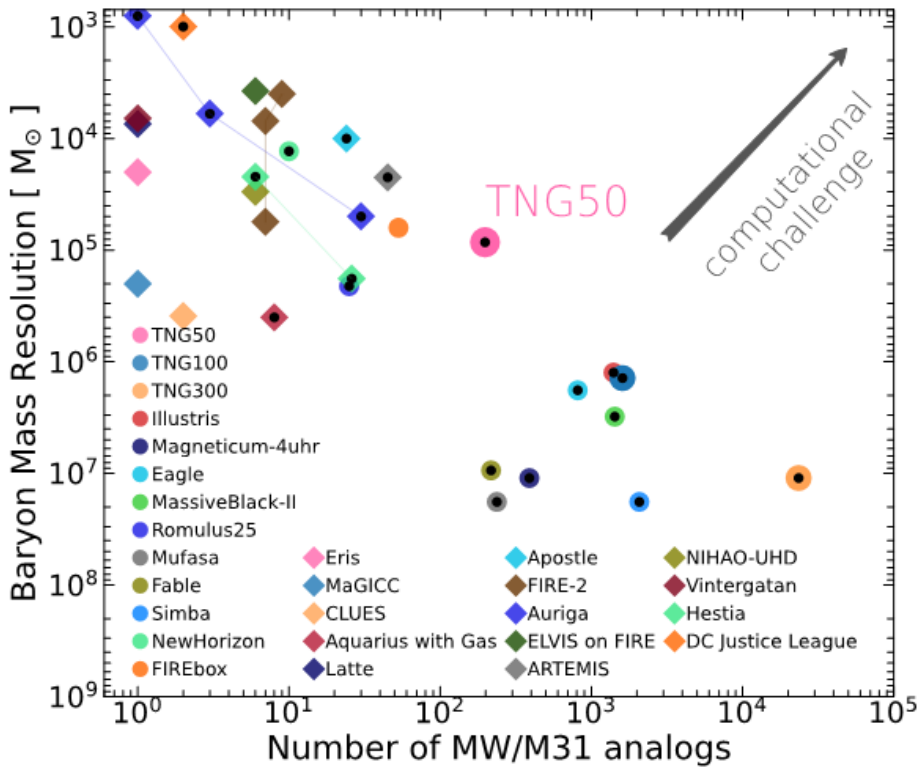

TNG100	2017	AREPO	unif.res.	yes	1606	1.4×10^6
TNG50	**2019**	**AREPO**	**unif.res.**	**yes**	**198**□	8.5×10^4

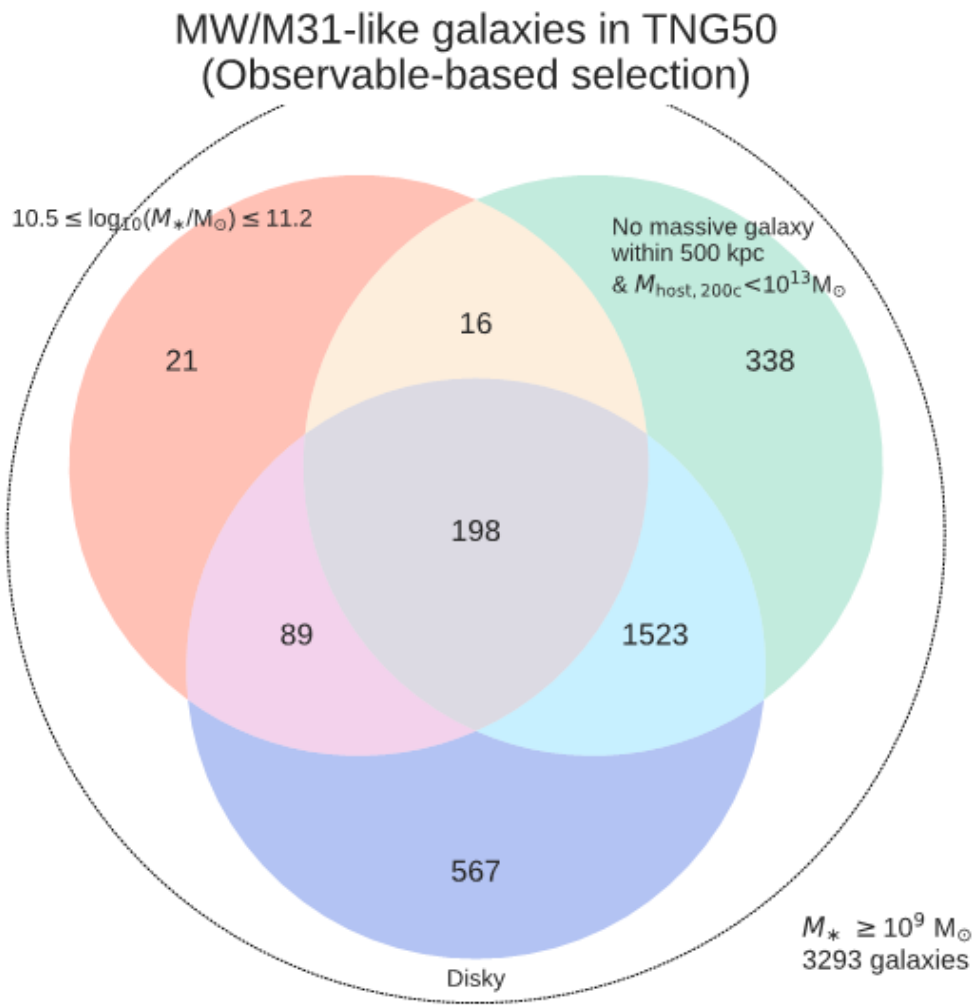

Figure 1. The landscape of ΛCDM cosmological simulations of MW/M31-like galaxies as of 2023. We contrast numerical projects in terms of baryonic mass resolution vs. number of simulated MW/M31 analogs. The TNG50 simulation this paper focuses on (magenta circle) is compared to state-of-the-art cosmological zoom-in simulations (diamonds) and so-called box or uniform-resolution large-volume simulations (circles): this comparison is deliberately similar to that in Fig. 1 of Nelson et al. (2019b) but focuses on MW/M31-

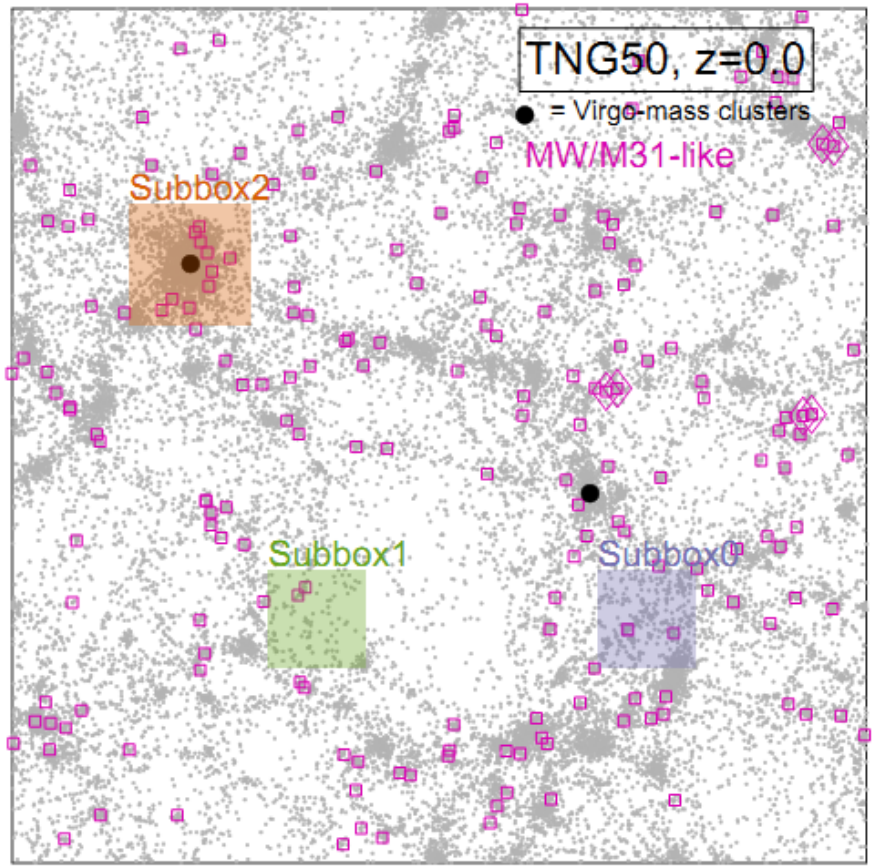

Figure 6. Location and large-scale environment of the 198 MW/M31-like galaxies (magenta) within the whole TNG50 simulated volume. The large-scale structure throughout the comoving volume of TNG50 (which spans about 52 comoving Mpc a side) is here depicted at $z = 0$ through the position of TNG50 galaxies more massive than 10^6 $M_\odot$ in stars (gray circles). This is a random projection, along the z-axis of the box, and also shows the location of the two Virgo-mass clusters in the simulation (large black circles). A handful of the selected objects are within the so-called Subboxes (shaded comoving cubes), whereby data is available every few million years (see Section A and Table A1). Three pairs compose Local-Group analogs (magenta diamonds).

Figure 2. Example galaxies from the TNG50 simulation at $z = 0$ with stellar mass and/or disk structure similar to the Milky Way or to Andromeda, among the 198 TNG50 MW/M31-like galaxies. These are shown in random projections, across 70 kpc a side, in a composite stellar light image of three HST/ACS bands (F435W, F606W, F775W; 0.049 arcsec/pixel) including radiative transfer in post-process with SKIRT (Camps & Baes 2015) and placing the galaxies at $z \sim 0.08$. A large gallery of all the TNG50 MW/M31-like galaxies can be found at https://www.tng-project.org/explore/gallery/pillepich23a.

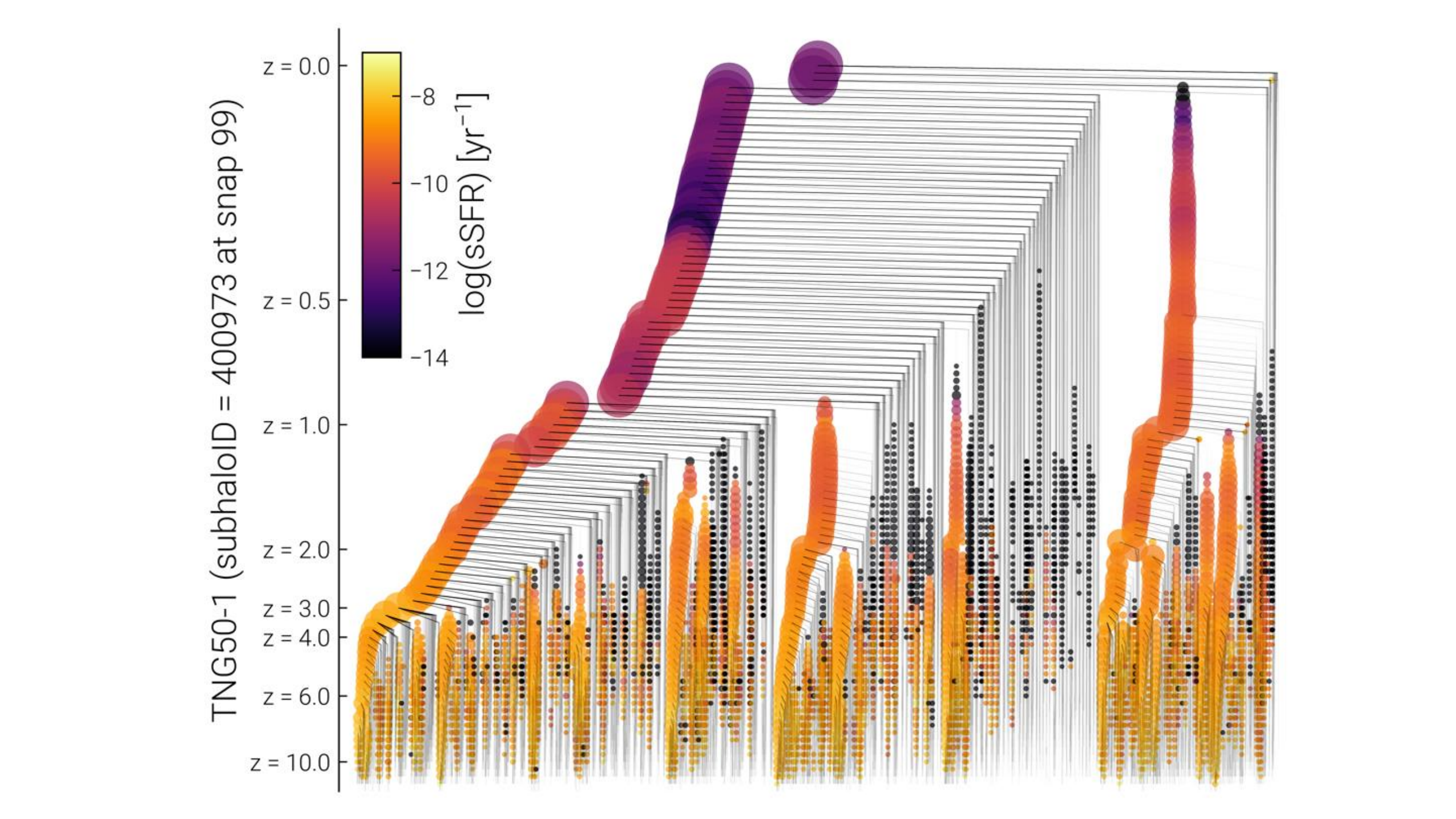
TNG50-1 (subhaloID = 400973 at snap 99)
z = 0.0
z = 0.5
z = 1.0
z = 2.0
z = 3.0
z = 4.0
z = 6.0
z = 10.0
log(sSFR) [yr^{-1}]
−8
−10
−12
−14

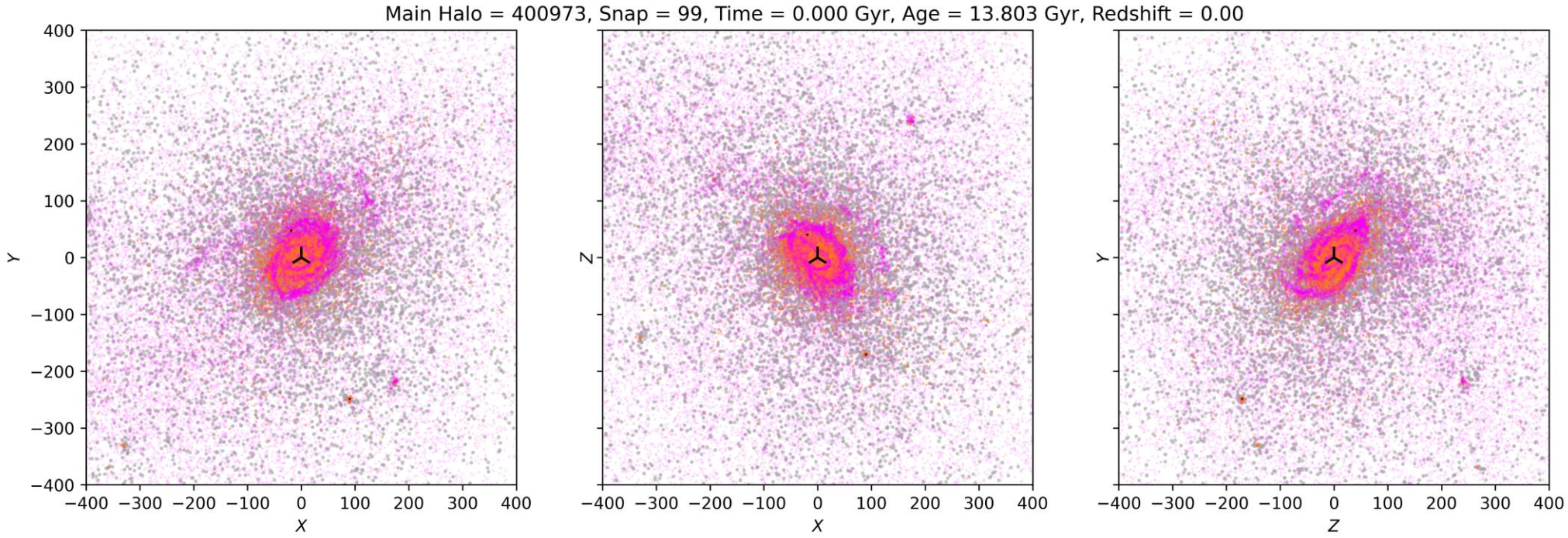
Main Halo = 400973, Snap = 99, Time = 0.000 Gyr, Age = 13.803 Gyr, Redshift = 0.00
Y
X
Z
X
Y
Z

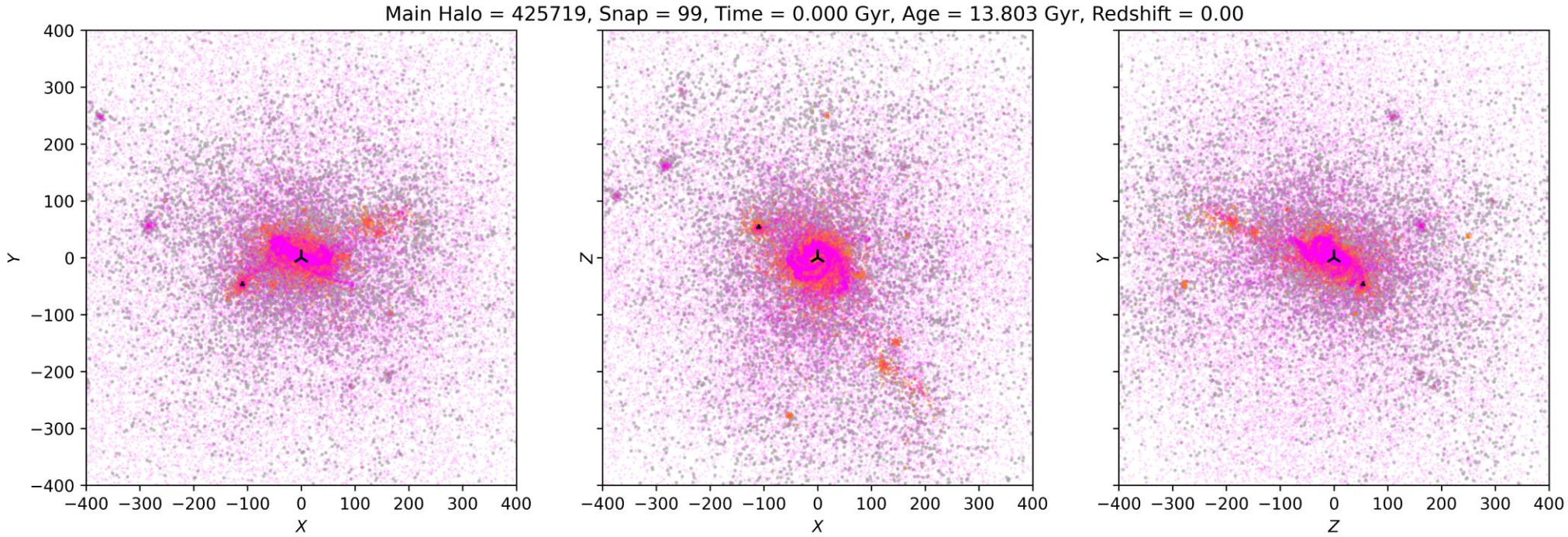
Main Halo = 425719, Snap = 99, Time = 0.000 Gyr, Age = 13.803 Gyr, Redshift = 0.00
Y
X
Z
X
Y
Z

Main Halo = 400973

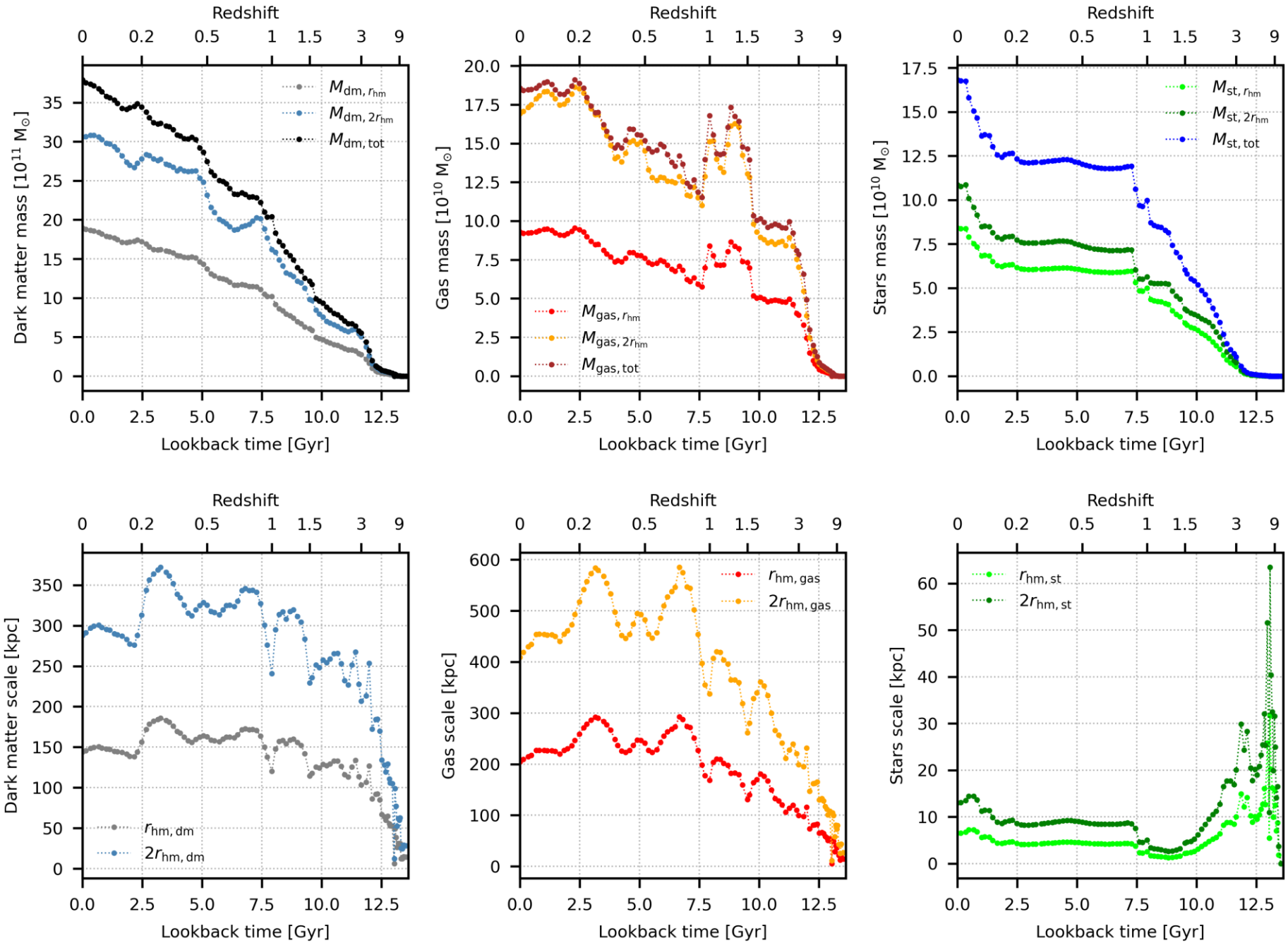

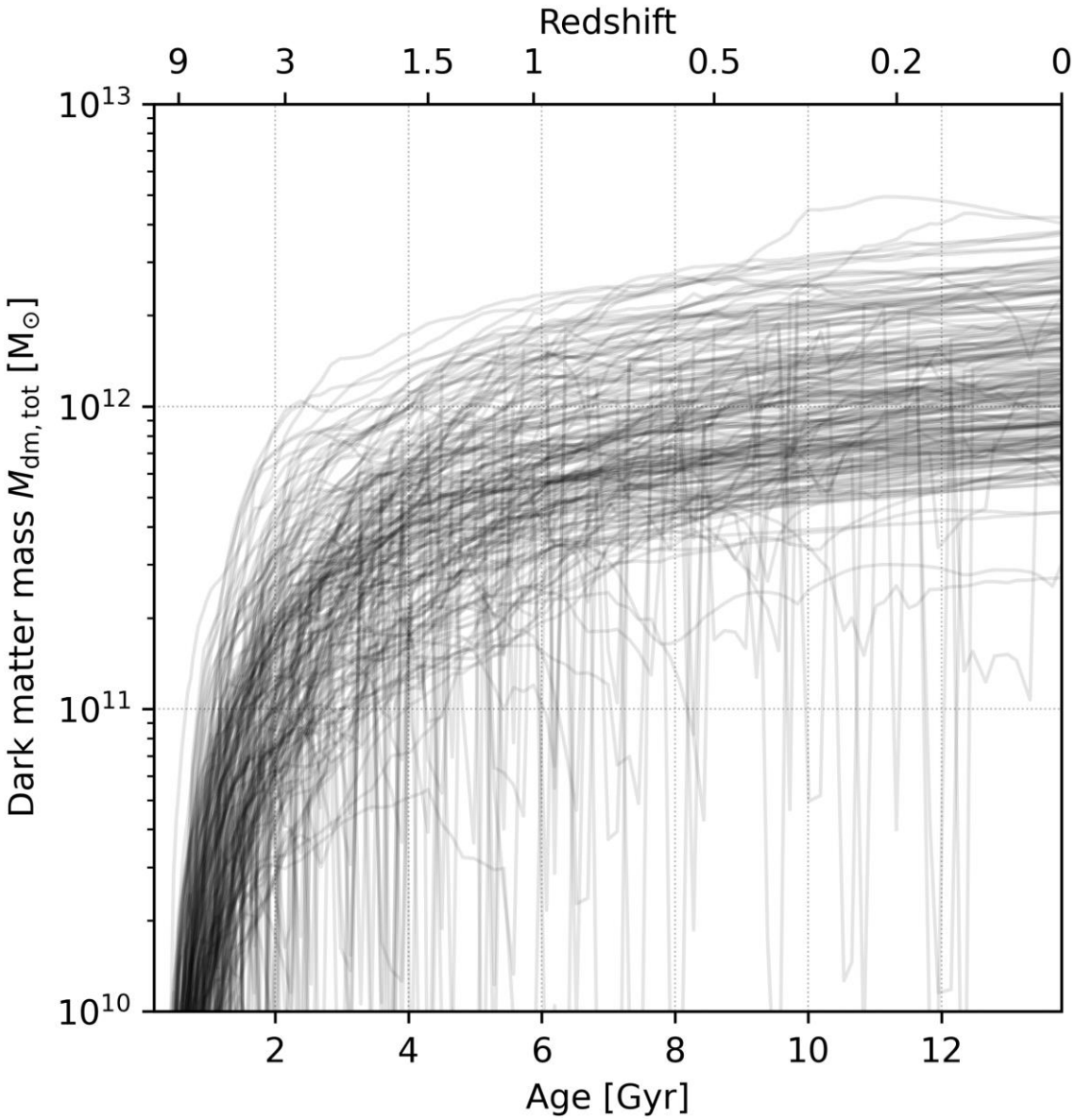
Redshift
9
3
1.5
1
0.5
0.2
0
10^{13}
10^{12}
10^{11}
10^{10}
Dark matter mass $M_{\mathrm{dm,\,tot}}$ [$M_\odot$]
2
4
6
8
10
12
Age [Gyr]

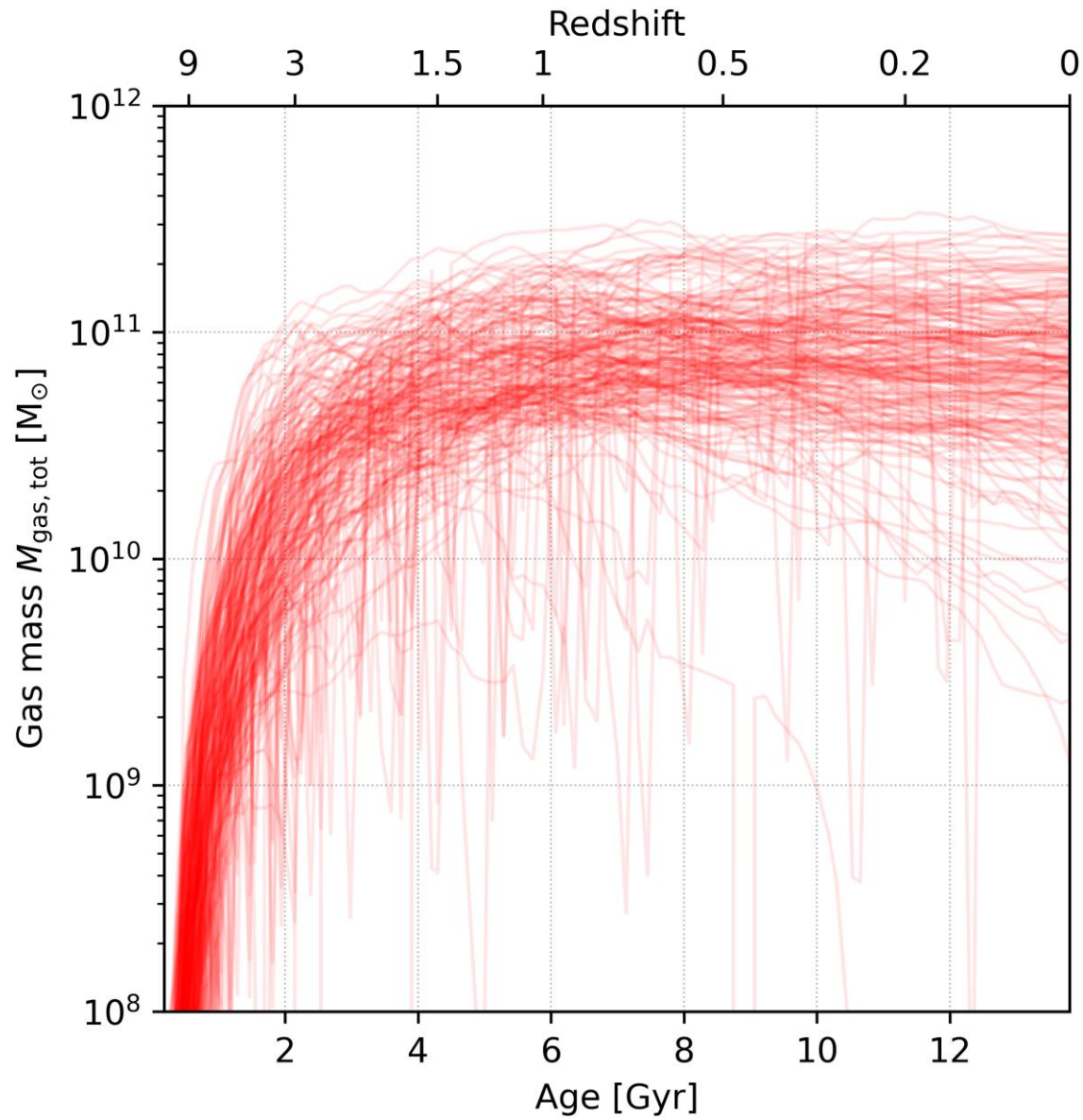
Redshift
9
3
1.5
1
0.5
0.2
0
10^{12}
10^{11}
10^{10}
10^{9}
10^{8}
Gas mass $M_{\mathrm{gas,\,tot}}$ [$M_\odot$]
2
4
6
8
10
12
Age [Gyr]

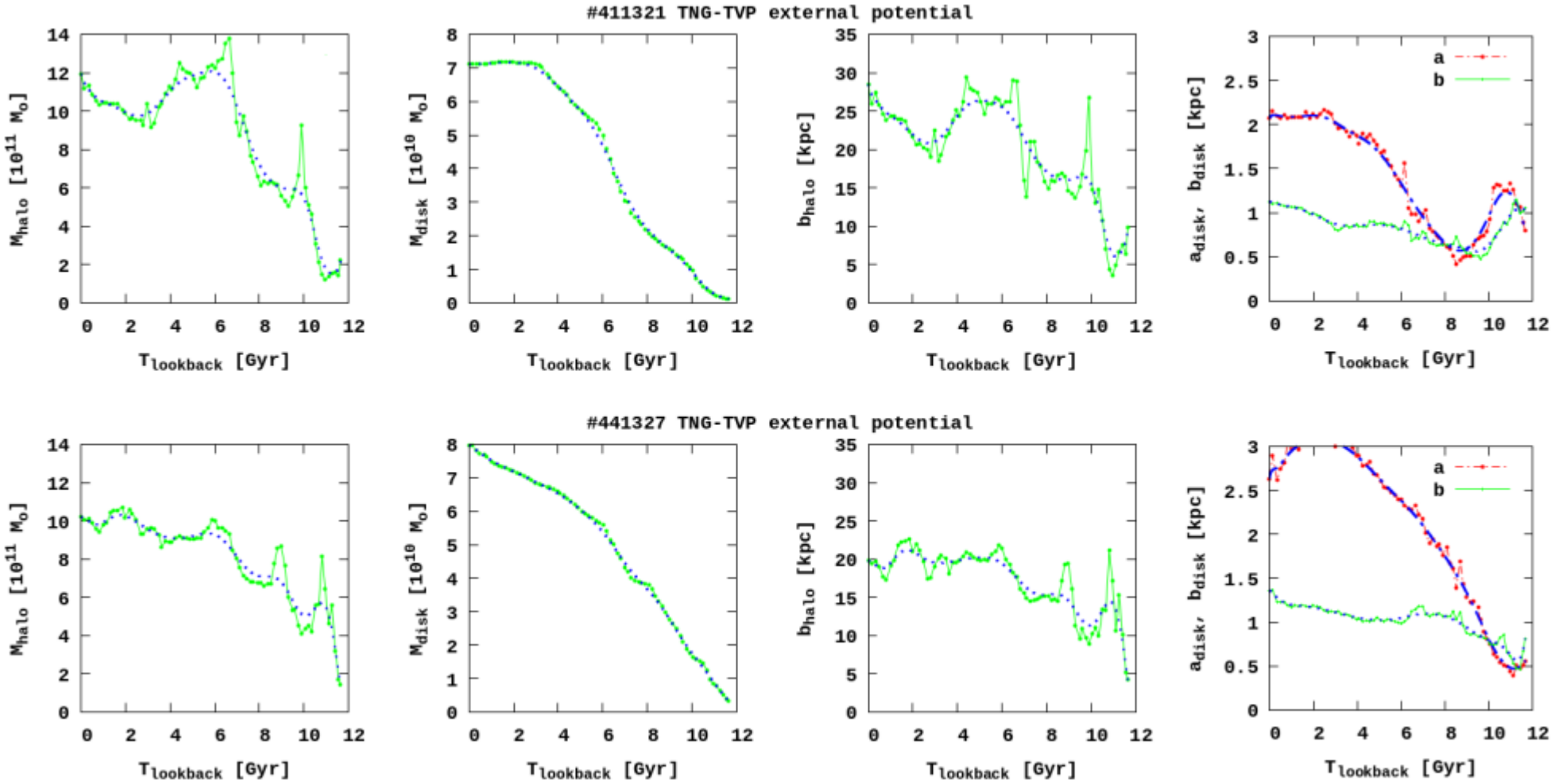

Mardini et al. 2020

https://github.com/Mohammad-Mardini/The-ORIENT

$$\Phi_{\rm tot} = \Phi_{\rm d}(R,z) + \Phi_{\rm h}(R,z) = $$

$$= -\frac{GM_{\rm d}}{\sqrt{R^2 + \left(a_{\rm d} + \sqrt{z^2 + b_{\rm d}^2}\right)^2}} - \frac{GM_{\rm h} \cdot \ln\left(1 + \frac{\sqrt{R^2+z^2}}{b_{\rm h}}\right)}{\sqrt{R^2+z^2}}, \quad (1)$$

Table 1. Parameters of the time-varying potentials selected from the IllustrisTNG-100 simulation at redshift zero. The last column shows the parameters of the corresponding MW components according to Bennett et al. (2022) at present.

Parameter	Unit	#411321	#441327	#451323	#462077	#474170	Milky Way
Disk mass, M_d	10^{10} $M_\odot$	7.110	7.970	7.670	7.758	5.825	6.788
Halo mass, M_h	10^{12} $M_\odot$	1.190	1.020	1.024	1.028	0.898	1.000
Disk scale length, a_d	1 kpc	2.073	2.630	2.630	1.859	1.738	3.410
Disk scale height, b_d	1 kpc	1.126	1.356	1.258	1.359	1.359	0.320
Halo scale height, b_h	10 kpc	2.848	1.981	2.035	2.356	1.858	2.770

Massari et al. 2019; Malhan et al. 2022

Armstrong et al. 2021; Haghi et al. 2015

Bajkova et al. 2021

https://bit.ly/3b0lafw

To transform the positions and velocities into the Cartesian galactocentric rest frame (see Johnson & Soderblom 1987; Bovy 2011, for the coordinate transformation equations), we assumed a galactocentric distance of the Sun $R_\odot$ = 8.178 kpc (Gravity Collaboration et al. 2019; Reid & Brunthaler 2004), a height above the Galactic plane $Z_\odot$ = 20.8 pc (Bennett & Bovy 2019), and the velocity of the local standard of rest (LSR) V_{LSR} = 234.737 km s^{-1} (Bovy et al. 2012; Drimmel & Poggio 2018). Accordingly, the Sun is located at $X_\odot$ = −8178 pc, $Y_\odot$ = 0 pc and $Z_\odot$ = 20.8 pc in our Cartesian galactocentric coordinate system. For the peculiar velocity of the Sun, we used the following values with respect to the LSR: $U_\odot$ = 11.1 km s^{-1}, $V_\odot$ = 12.24 km s^{-1}, and $W_\odot$ = 7.25 km s^{-1} (Schönrich et al. 2010).

https://people.smp.uq.edu.au/HolgerBaumgardt/globular/orbits_table.txt

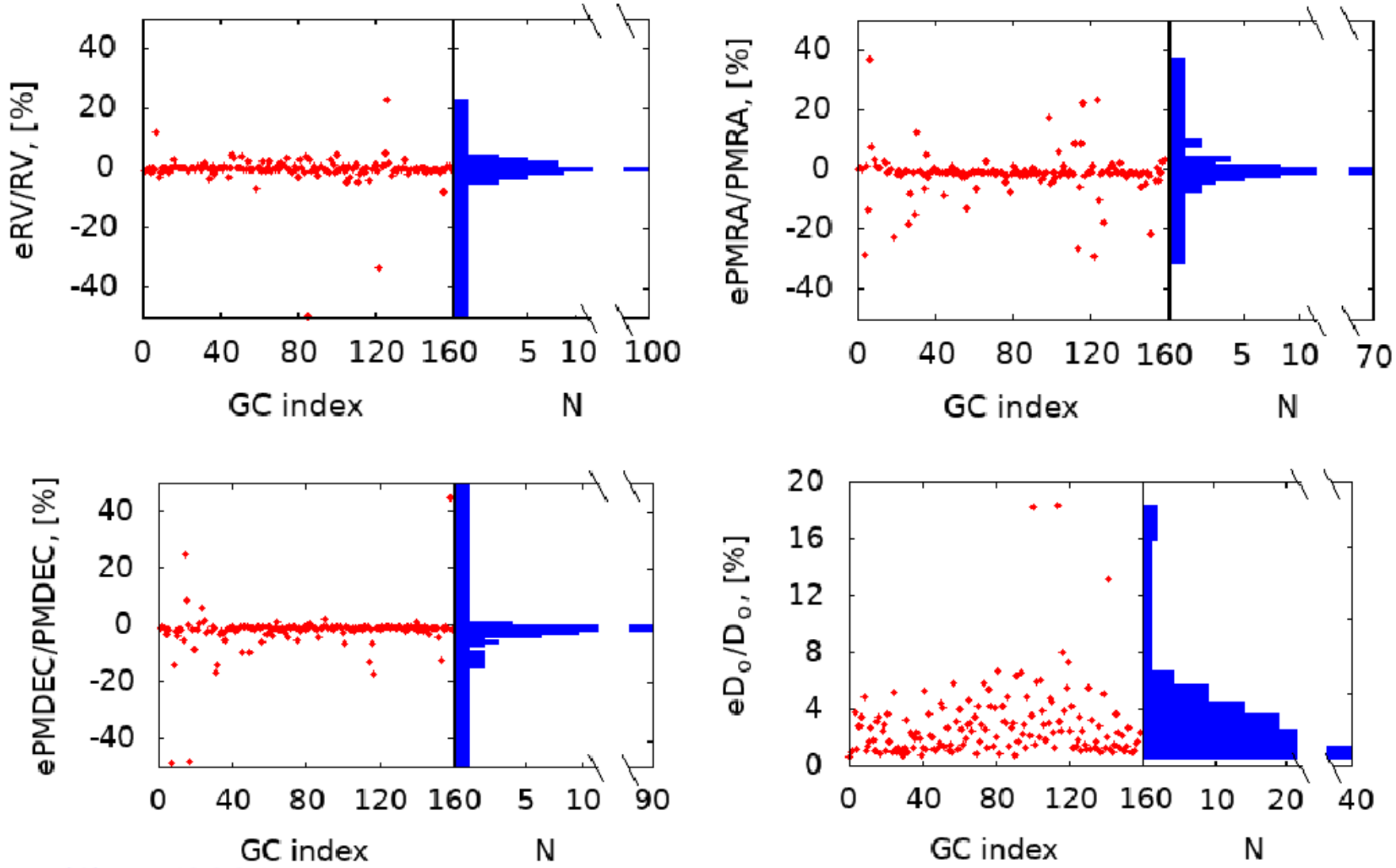

Baumgardt & Vasiliev (2021)

Fig. 1. Distribution of the relative errors *(from left to right)*: Radial velocity (eRV), proper motions in right ascension (ePMRA), and declination (ePMDEC), and in heliocentric distance $eD_{\odot}$. Blue histograms represent the error distributions. The following GCs are not shown because the error values are too high: Crater, Lae 3, NGC 6760, BH 261, NGC 6553, and Pal 13, except in the graph in the bottom right panel.

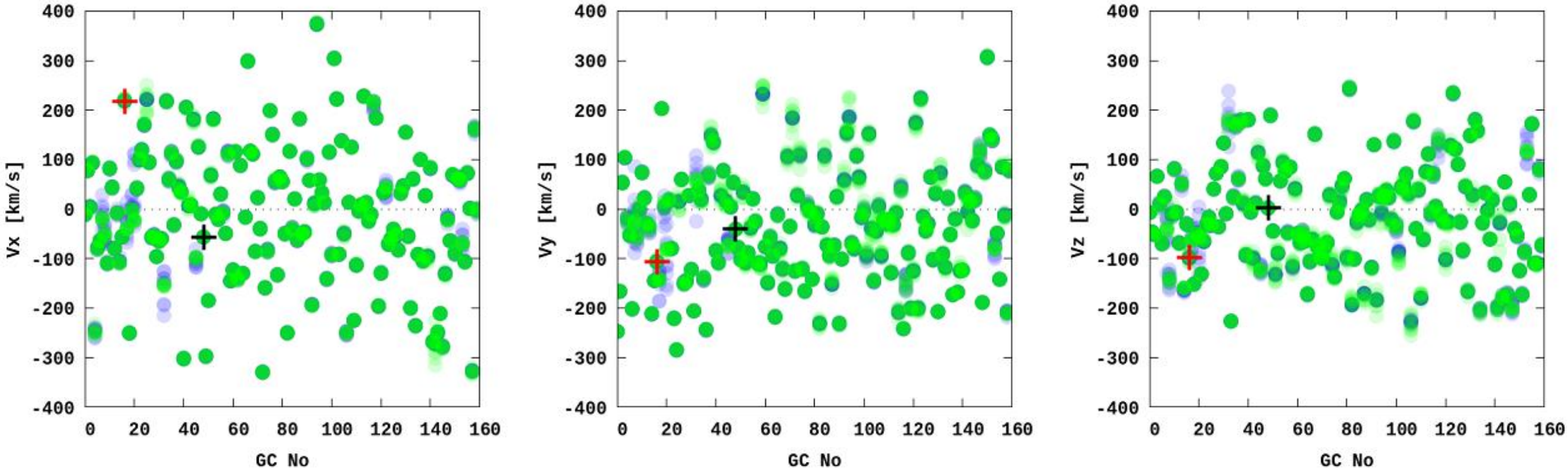

Fig. 3. Influence of the error randomisation on the initial velocity components in the galactocentric Cartesian reference frame. The distance determination is shown by green circles and the velocity determination by blue circles. The red cross marks Crater, and the black cross indicates NGC 6121.

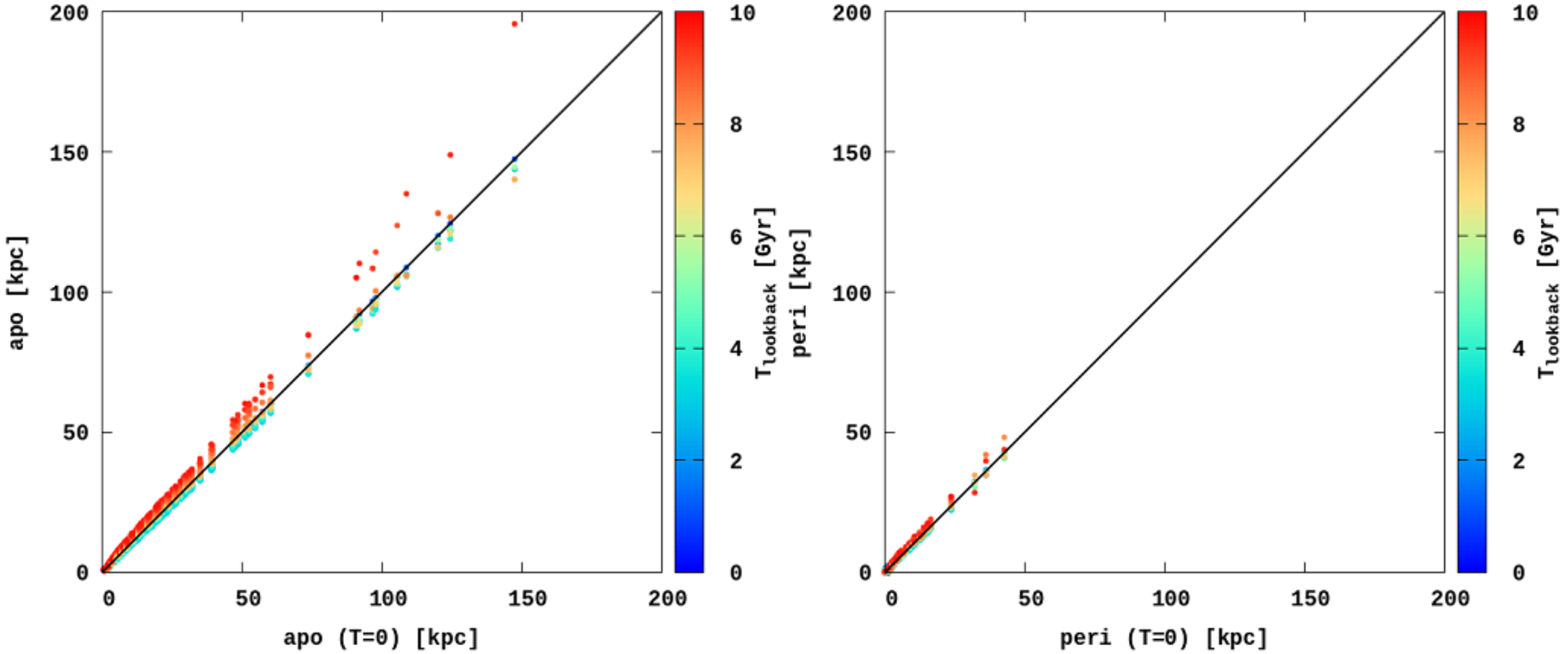

Fig. 7. Evolution of the apocenters (*left panel*) and pericenters (*right panel*) for the 159 GCs in the 411321 TNG-TVP. The colour-code corresponds to the lookback time.

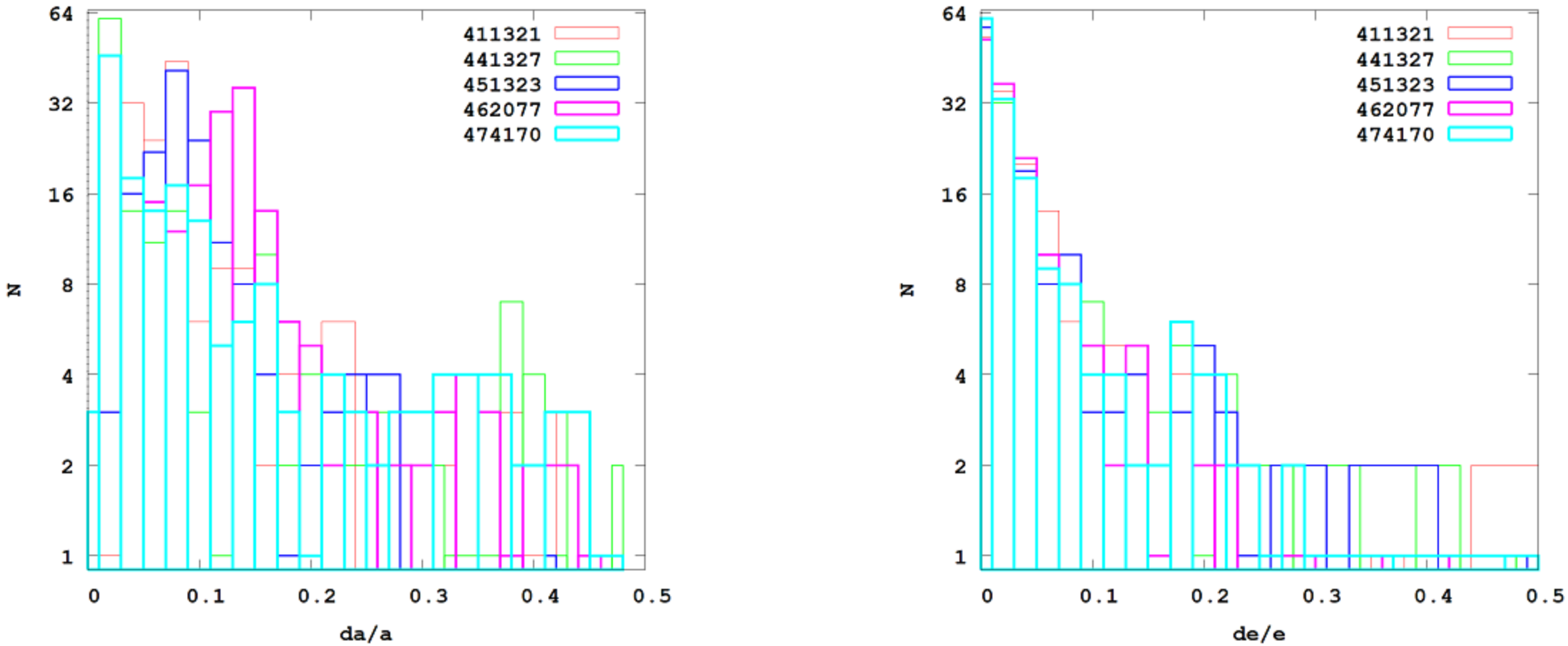

Fig. 5. Relative orbital semi-major $\Delta a/a$ (left) and eccentricity $\Delta e/e$ (right) changes during the GC orbital evolution for all five TNG-TVPs.

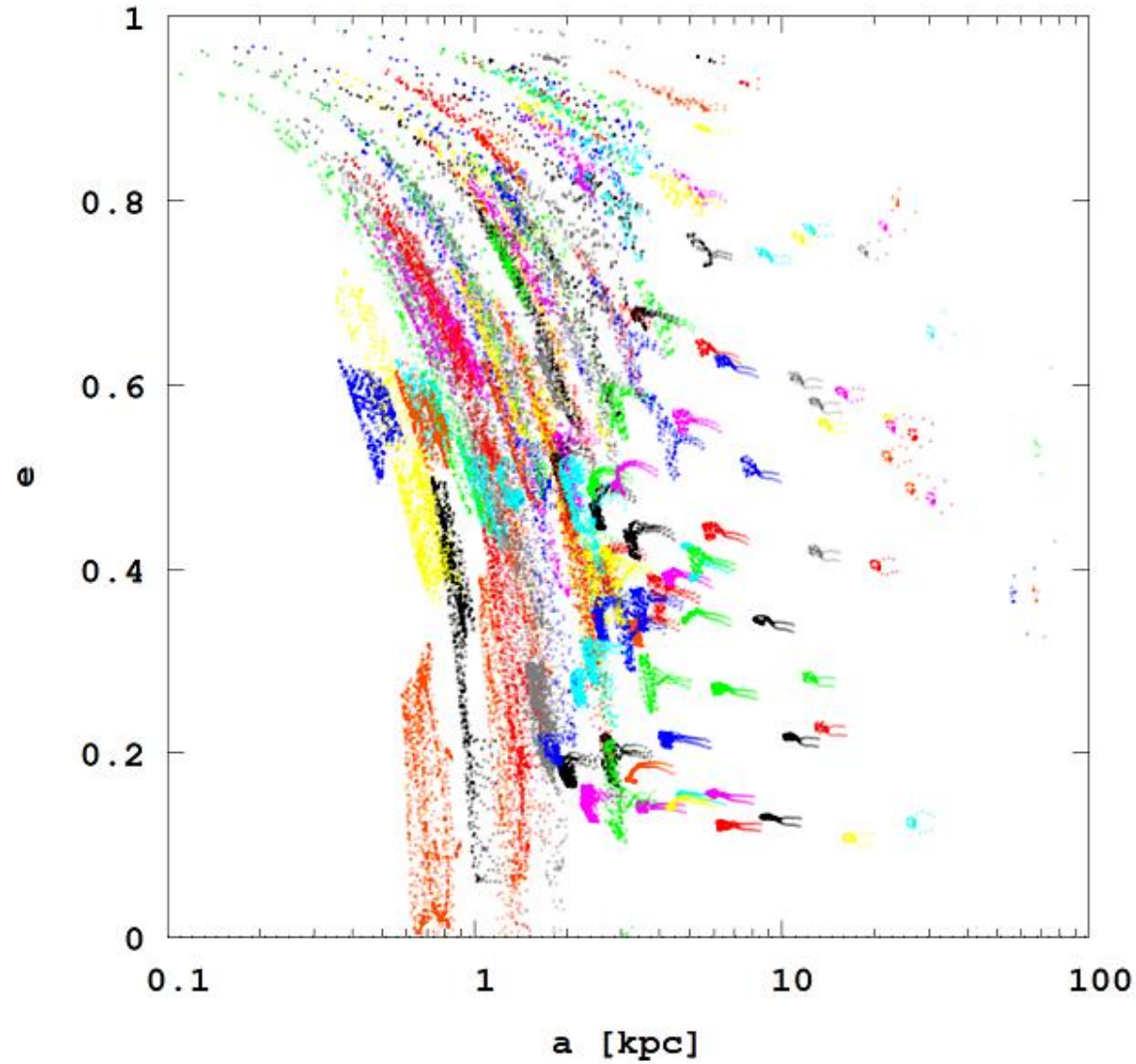

Fig. 6. Evolution of the GC orbital semi-major and eccentricity during the whole backward integration time in the case of 411321 TNG-TVP. The inner GCs (a ≤3 kpc) have more regular and larger eccentricity changes during the evolution. The outer GCs (a >3 kpc) have much smaller eccentricity changes during the whole backward integration time.

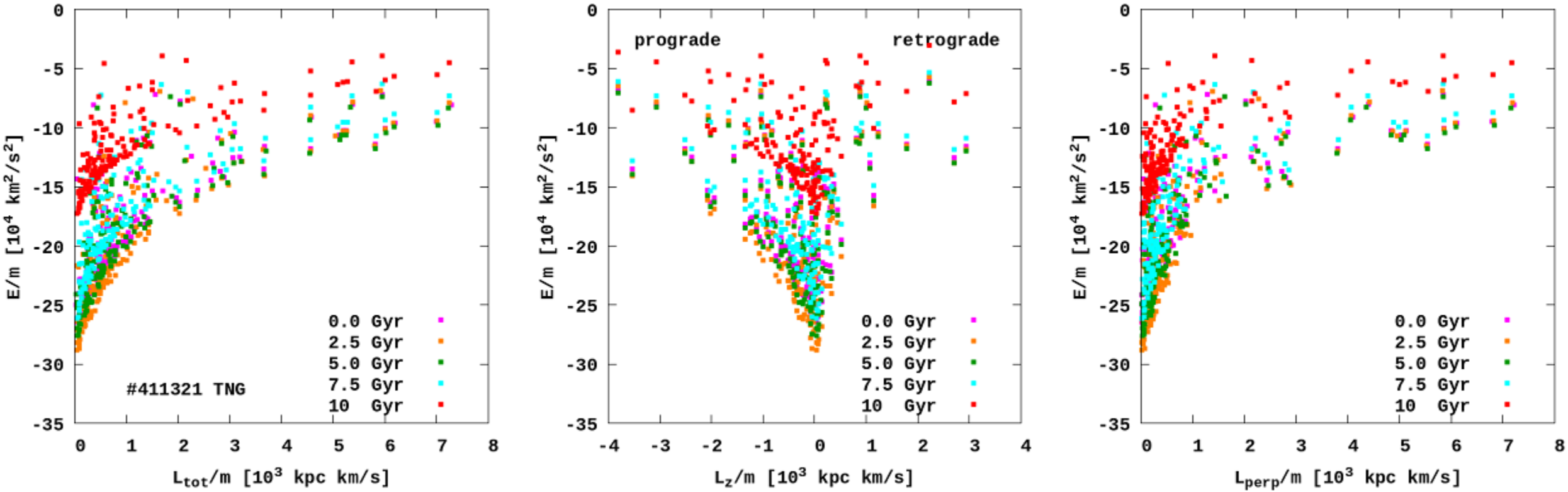

Fig. 14. Evolution of the total angular momentum vs energy phase space ($L_{\rm tot}$, E) *(left panels, top to bottom)*, zth component of the angular momentum vs energy (L_z, E) *(middle, top to bottom),* and the perpendicular component of the angular momentum vs energy ($L_{\rm perp}$, E) *(right, top to bottom)* for 411321, 441327, and 451323 TNG-TVPs. The colours represent data at different times in Gyr lookback time: magenta for $T = 0$, orange for $T = 2.5$, green for $T = 5$, cyan for $T = 7.5$, and red for $T = 10$. The GCs Pal 3, Crater, and Sagittarius II are not shown in the ($L_{\rm tot}$, E) and ($L_{\rm perp}$, E) phase spaces, and Sagittarius II is not shown in (L_z, E) phase space because their values are extremely high.

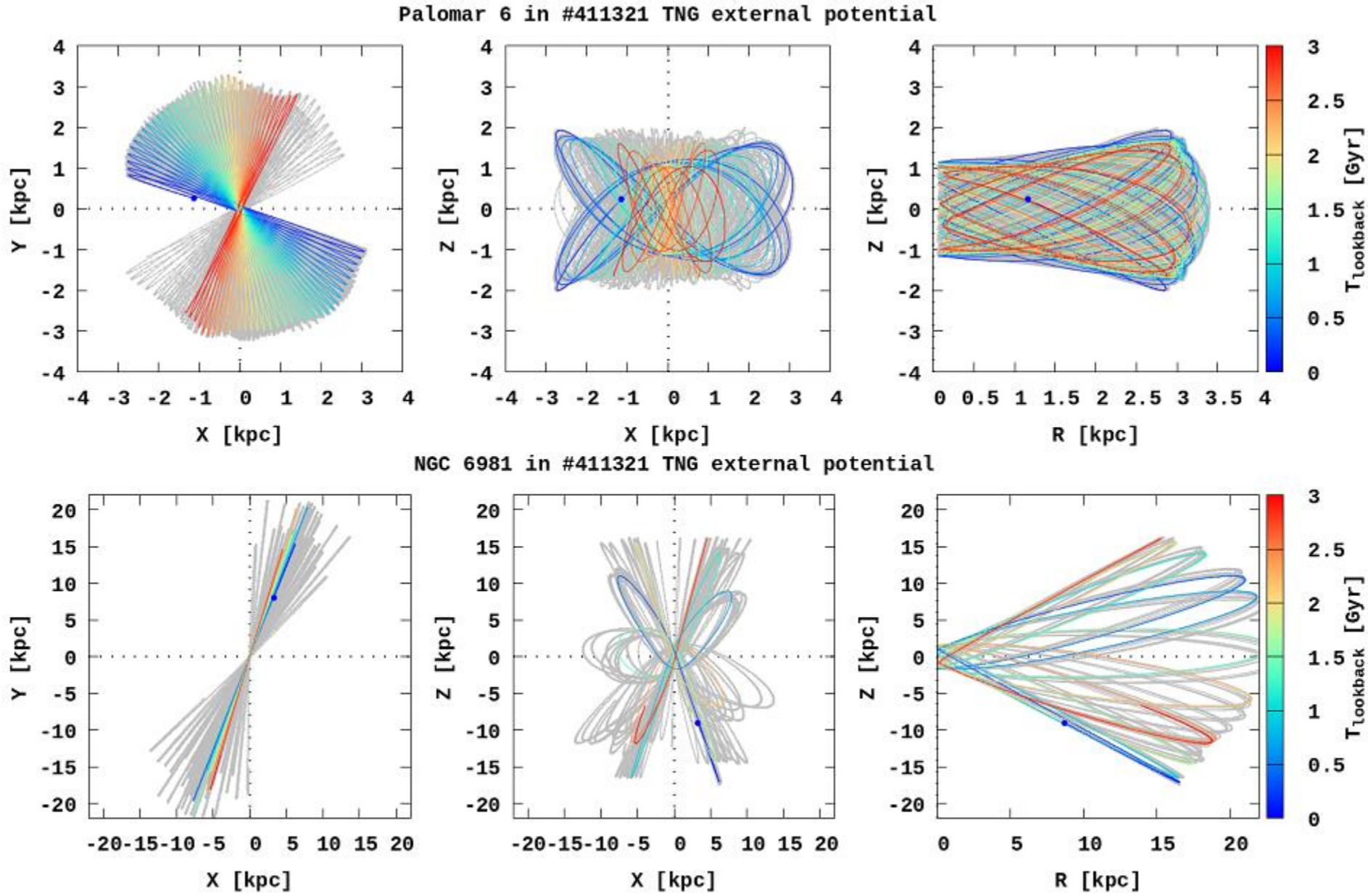

Fig. 1. Orbital evolution of two selected clusters: Pal 6 and NGC 6981. On the plot we show only the first 3 Gyr evolution in #411321 TNG-TVP external potential. The colour-coded line presents the orbit based on catalogue initial positions and velocities. The grey colour represents the orbits for ten different random realisations of initial data.

$$\frac{dN_{\mathrm{GalC}}(D_{\mathrm{m}})}{dt} = 10^{\mathrm{a}\cdot\lg(D_{\mathrm{m}})+\mathrm{b}},$$

Table 2. Fitting parameters for the interaction rate GC with GalC as a function of the relative distance from the centre for four TNG-TVP external potentials.

Potential	a	b
#411321	3.073 ± 0.588	-5.181 ± 1.205
#411321-m*	3.183 ± 0.609	-5.404 ± 1.247
#441327	3.202 ± 0.584	-5.519 ± 1.187
#451323	2.563 ± 0.328	-3.900 ± 0.670
#462077	2.897 ± 0.594	-4.867 ± 1.218
Mean	2.934 ± 0.524	-4.867 ± 1.070

Notes. * simulations for which additional SMBH mass has been taken into account. This value was not used for the mean calculation.

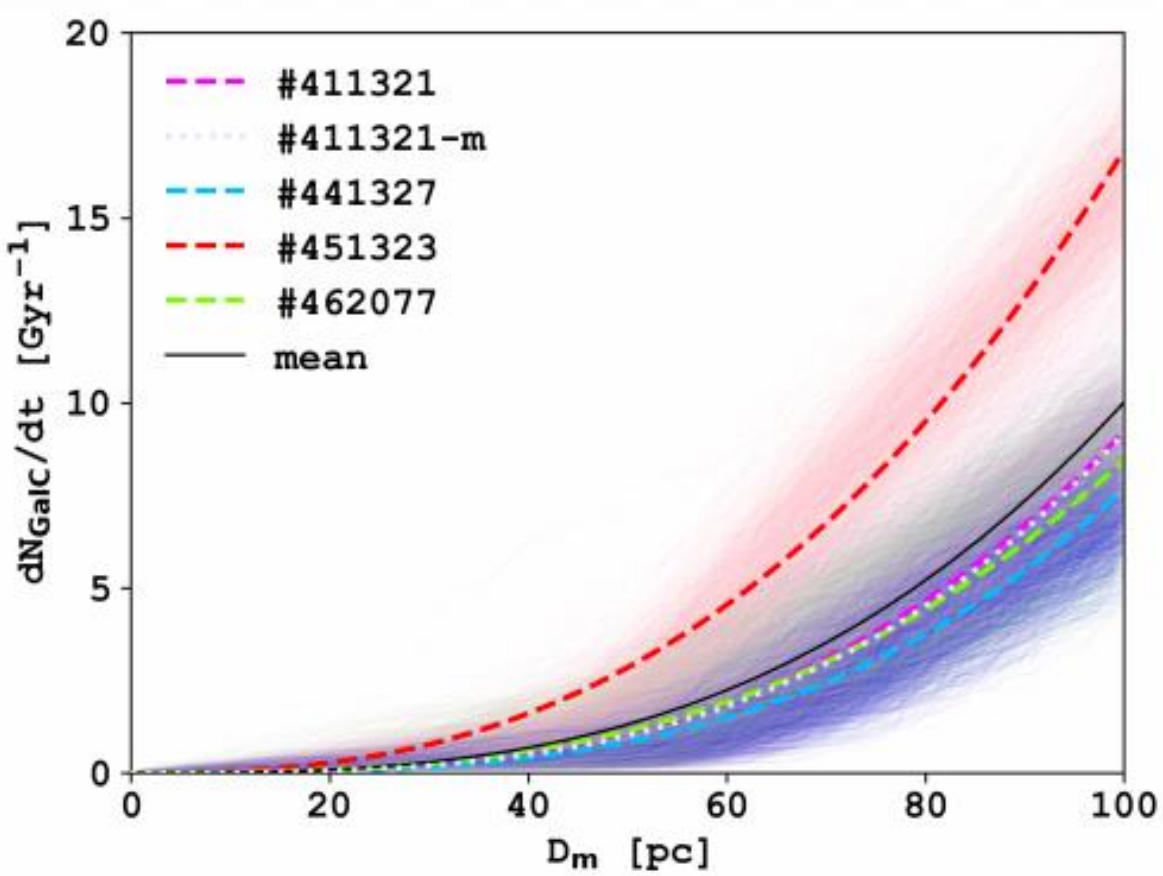

Fig. 2. Interaction rate of the GCs with GalC as a function of the relative distance from the centre for the five TNG-TVP external potentials and 1000 random realisations (thin solid coloured lines). Thick dashed lines are a power-law fit in TNG potentials. The solid black line is a mean fitting line (see Table 2). The pale violet dotted line is a power-law fit for potential #411321-m for which the SMBH mass has been taken into account.

Table 3. Percent of probability of the GCs' interaction with the GalC in all 1000 sets of randomisation for four TNG TVPs.

GC	#411321	#411321-m	#441327	#451323	#462077	Mean
(1)	(2)	(3)	(4)	(5)	(6)	(7)
NGC 6401	100.0	99.9	100.0	100.0	100.0	100.0
Pal 6	100.0	99.6	99.9	100.0	100.0	99.9 ± 0.1
NGC 6681	99.9	99.9	100.0	100.0	100.0	99.9 ± 0.1
NGC 6712	99.9	100.0	99.9	99.8	100.0	99.9 ± 0.1
NGC 6287	100.0	100.0	100.0	97.0	92.1	97.3 ± 3.7
NGC 6642	99.8	99.8	99.3	100.0	99.5	99.7 ± 0.3
NGC 6981	83.9	84.9	90.2	93.5	87.8	88.9 ± 4.0
HP 1	98.7	99.0	70.7	99.5	83.0	89.9 ± 13.8
NGC 1904	72.4	73.0	73.6	83.2	76.7	76.5 ± 4.8
NGC 362	24.4	27.9	30.7	41.2	12.9	27.3 ± 11.8

Notes. Column (1) – name of a GC. Columns (2)–(6) – interaction probabilities for GCs with the GalC for each TNG-TVP external potential in percent. `#411321-m` – the special potential with the MW SMBH mass. Column (7) – the average probability value with error over all potentials, excluding the `#411321-m` potential.

Table 4. Statistics of the characteristics of the GCs' interaction with the GalC in all four TNG-TVP external potentials.

Pot / GC	#411321			#411321-m		
	$< D_m >$ pc	$< dV >$ km s^{-1}	$< N_{int} >$	$< D_m >$ pc	$< dV >$ km s^{-1}	$< N_{int} >$
NGC 6401	56 ± 10	331 ± 18	19 ± 2	58 ± 10	333 ± 17	18 ± 4
Pal 6	58 ± 12	340 ± 10	11 ± 6	58 ± 13	341 ± 10	10 ± 5
NGC 6681	42 ± 16	410 ± 4	3 ± 1	45 ± 17	411 ± 1	3 ± 1
NGC 6712	52 ± 8	379 ± 10	8 ± 2	53 ± 8	380 ± 10	8 ± 2
NGC 6287	82 ± 5	405 ± 10	4 ± 1	81 ± 4	398 ± 11	4 ± 1
NGC 6642	62 ± 16	262 ± 19	27 ± 10	63 ± 14	260 ± 19	28 ± 9
NGC 6981	57 ± 24	545 ± 8	2 ± 1	57 ± 24	547 ± 8	2 ± 1
HP 1	50 ± 21	304 ± 10	11 ± 4	50 ± 22	306 ± 11	16 ± 4
NGC 1904	53 ± 25	517 ± 17	3 ± 2	54 ± 24	518 ± 18	3 ± 1
NGC 362	88 ± 10	484 ± 6	1 ± 1	87 ± 10	481 ± 5	1 ± 1

Pot / GC	#441327			#451323			#462077		
	$< D_m >$ pc	$< dV >$ km s^{-1}	$< N_{int} >$	$< D_m >$ pc	$< dV >$ km s^{-1}	$< N_{int} >$	$< D_m >$ pc	$< dV >$ km s^{-1}	$< N_{int} >$
NGC 6401	48 ± 7	352 ± 12	38 ± 6	50 ± 7	366 ± 19	20 ± 3	54 ± 10	305 ± 12	14 ± 3
Pal 6	58 ± 9	359 ± 15	22 ± 4	70 ± 8	351 ± 29	10 ± 4	65 ± 9	299 ± 7	10 ± 3
NGC 6681	25 ± 10	440 ± 14	13 ± 2	34 ± 13	439 ± 14	7 ± 1	21 ± 11	368 ± 5	7 ± 2
NGC 6712	49 ± 10	427 ± 16	13 ± 3	54 ± 6	382 ± 25	8 ± 3	59 ± 10	342 ± 6	7 ± 2
NGC 6287	94 ± 4	409 ± 11	2 ± 1	84 ± 7	418 ± 20	2 ± 1	77 ± 3	375 ± 4	4 ± 2
NGC 6642	51 ± 13	300 ± 10	44 ± 7	59 ± 22	276 ± 27	25 ± 13	66 ± 13	226 ± 13	20 ± 6
NGC 6981	46 ± 24	590 ± 14	3 ± 1	51 ± 24	540 ± 28	3 ± 1	48 ± 24	511 ± 12	3 ± 1
HP 1	46 ± 21	327 ± 14	16 ± 6	65 ± 23	290 ± 2	4 ± 2	61 ± 25	282 ± 5	7 ± 4
NGC 1904	51 ± 25	588 ± 19	4 ± 2	54 ± 25	539 ± 47	3 ± 1	57 ± 25	500 ± 9	3 ± 1
NGC 362	85 ± 11	530 ± 12	2 ± 1	88 ± 10	482 ± 10	1 ± 1	87 ± 10	457 ± 6	1 ± 1

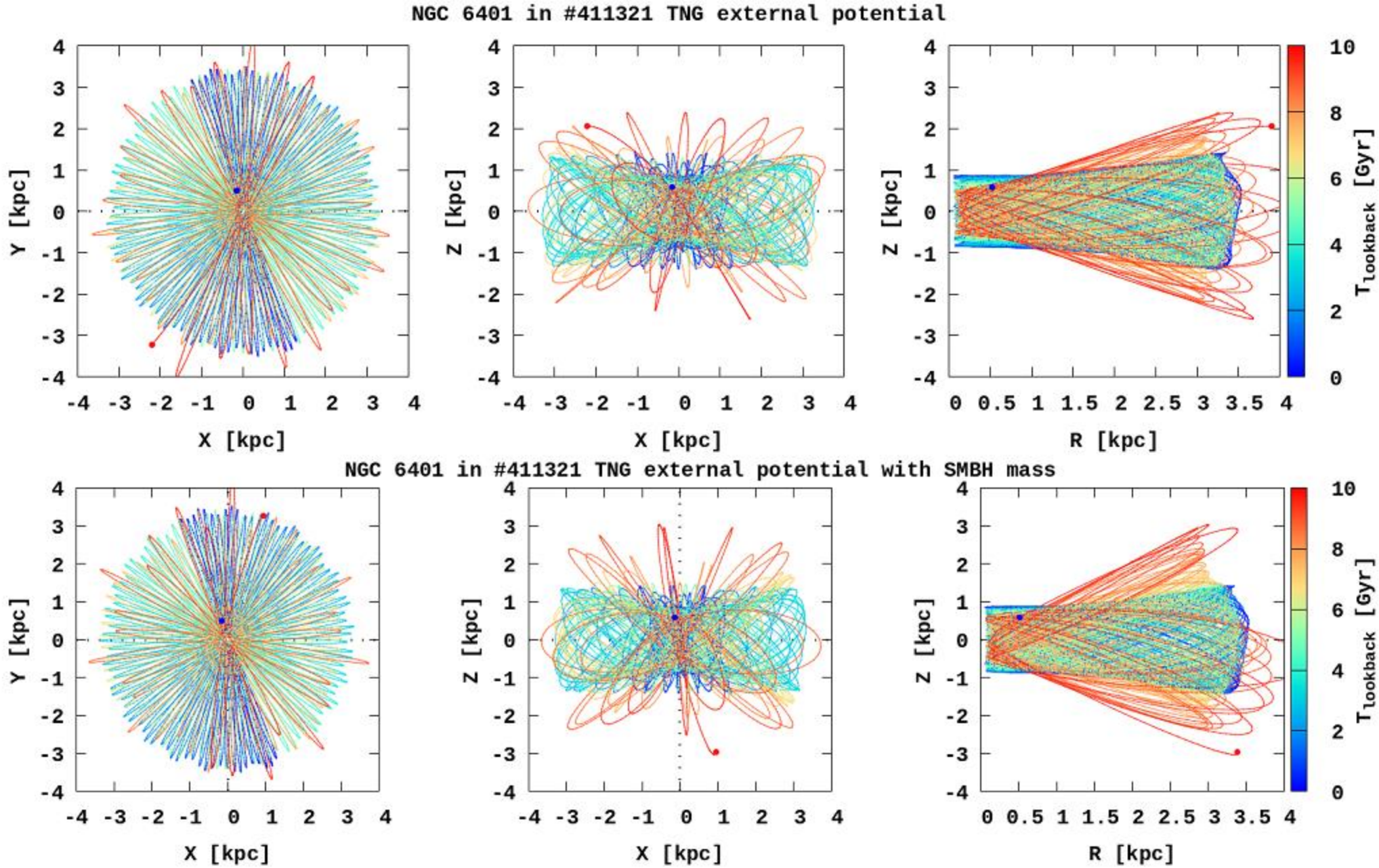
NGC 6401 in #411321 TNG external potential
Y [kpc]
X [kpc]
Z [kpc]
X [kpc]
Z [kpc]
R [kpc]
T_lookback [Gyr]
NGC 6401 in #411321 TNG external potential with SMBH mass
Y [kpc]
X [kpc]
Z [kpc]
X [kpc]
Z [kpc]
R [kpc]
T_lookback [Gyr]

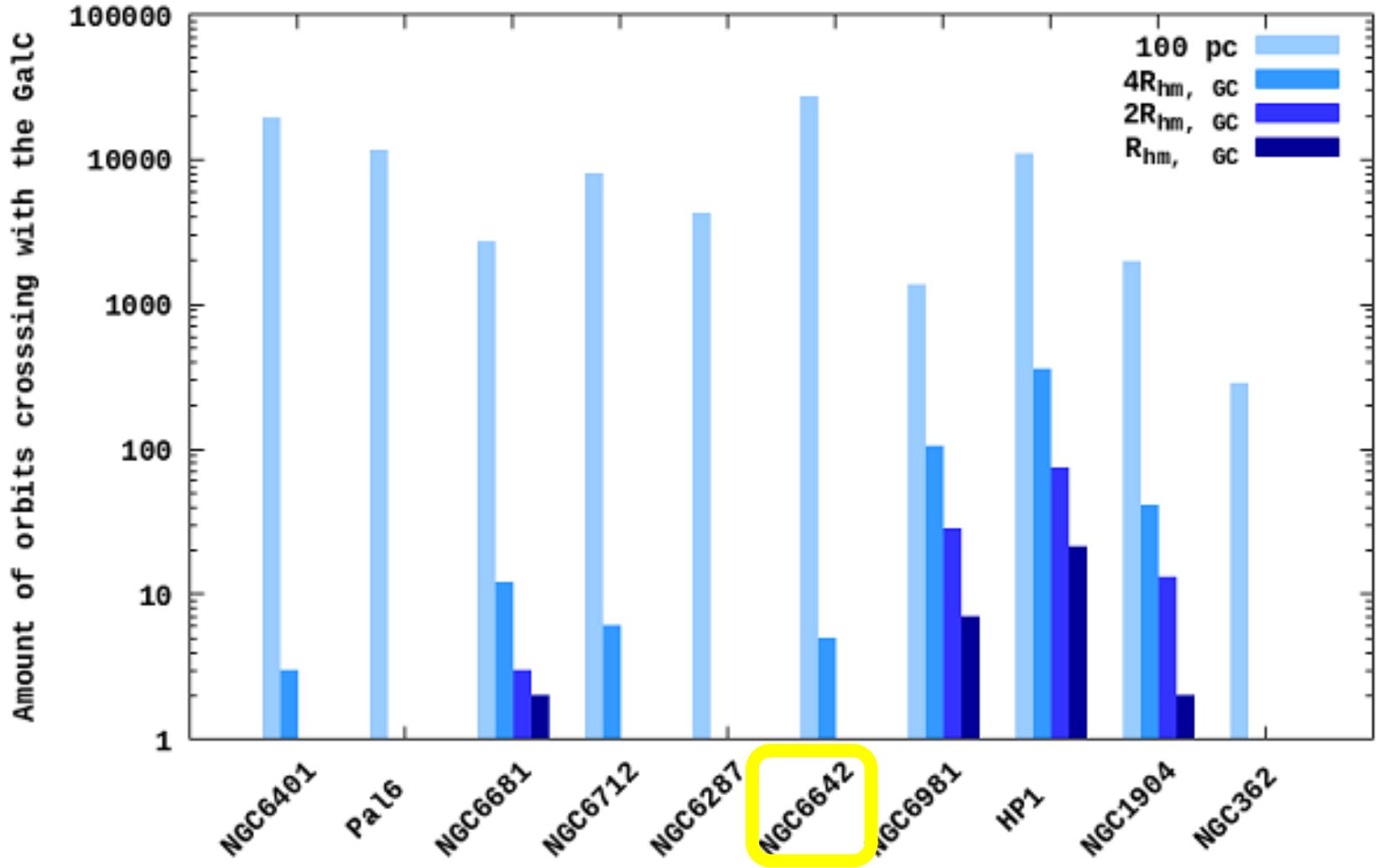

Fig. 1. Amount of orbits crossings with the GalC for selected GCs for four different distance criteria in 411321 TNG-TVP external potential.

Table 2. Initial kinematics and physical characteristics at eight billion years lookback time for GCs.

GC	X	Y	Z	V_x	V_y	V_z	E/m	$L_{\rm tot}/M$	M	N	$r_{\rm hm}$	W_0
	pc	pc	pc	km s^{-1}	km s^{-1}	km s^{-1}	10^4 km^2 s^{-2}	10^2 kpc km s^{-1}	10^6 M$_\odot$		pc	
(1)	(2)	(3)	(4)	(5)	(6)	(7)	(8)	(9)	(10)	(11)	(12)	(13)
NGC 6401	-1493	-3213	398	5	-3	-57	-18.8	2.03	1.2	2 249640	6.5	9
Palomar 6	1499	465	-1655	140	51	-81	-18.8	1.14	1.0	1 751 970	3.5	9
NGC 6681	1392	-4638	4243	-0.7	-1	61	-16.6	2.9	1.3	2 265 380	3.0	8
NGC 6642	983	-897	545	-47	54	-117	-21.2	1.1	1.5	2 613 856	4.0	9
NGC 6981	1774	4001	-4943	70	159	-270	-11.5	3.7	1.0	1 742 560	7.0	9
HP 1	-580	242	1859	71	-36	128	-19.5	2.3	1.3	2 265 340	6.0	8

Notes. Column (1) – the GCs names; columns (2) – (4) – initial position in Cartesian Galactocentric frame; columns (5) – (7) – initial velocities in Cartesian Galactocentric frame; column (8) – total specific energy; column(9) – total specific angular momentum; column (10) – initial mass; column (11) – initial number of stars; column (12) – initial radius of half-mass; column (13) – initial concentration of King profile.

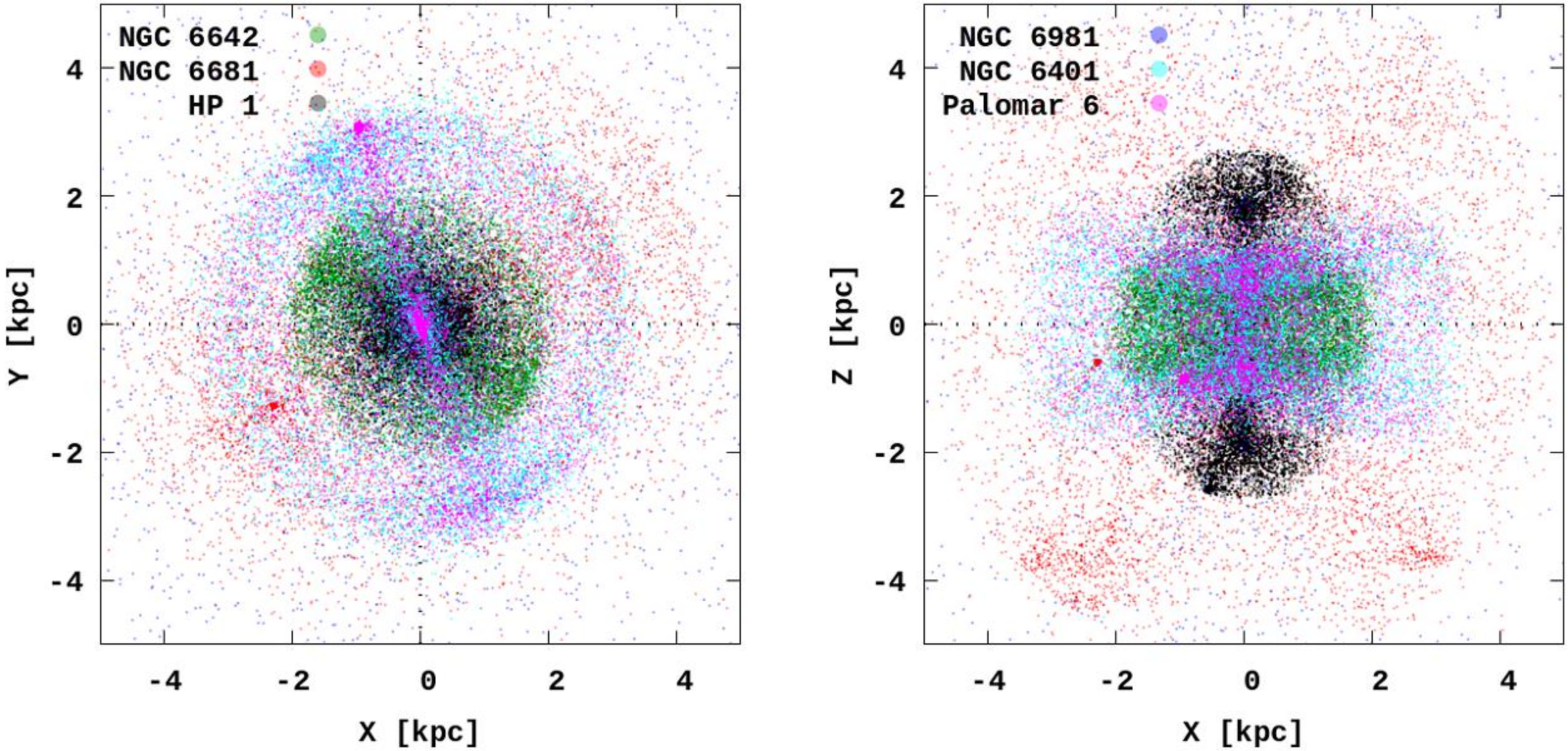

Fig. 8. Positions of the stars for six GCs in the central region of the Galaxy at present time.

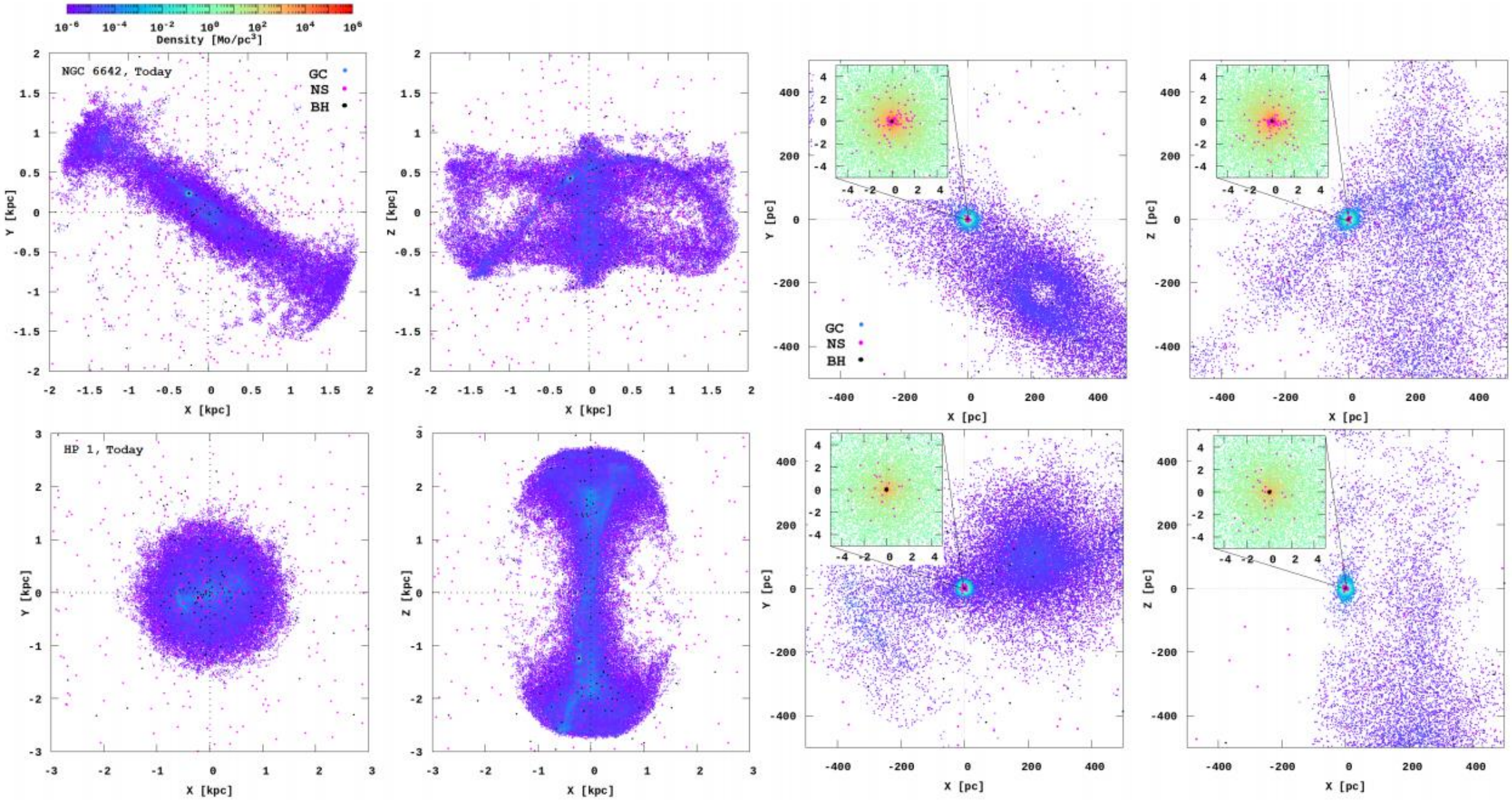

Fig. 9. NGC 6642 and HP 1 clusters today density distributions in 411321 TNG-TVP external potential. The orbital global evolution is present in two planes (X,Y) and (X,Z), *left panels*. GC central part in local frame with the BHs (black dots), NSs (magenta dots) and with detail central area (with box size 10 pc) we present in *two right panels*.

Table 3. Masses inside r_{hm} and r_{tid} for today, according to the numerical modelling.

GC	r_{hm} pc	r_{tid} pc	$M(r_{hm})$ 10^4 $M_\odot$	$M(r_{tid})$ 10^4 $M_\odot$
NGC 6401	4.3	28	7.1	14.2
Palomar 6	2.7	70	7.6	15.2
NGC 6681	4.5	37	18.5	37.0
NGC 6642	1.5	11	8.2	16.6
NGC 6981	8.9	215	10.4	15.9
HP 1	4.0	37	7.0	14.2

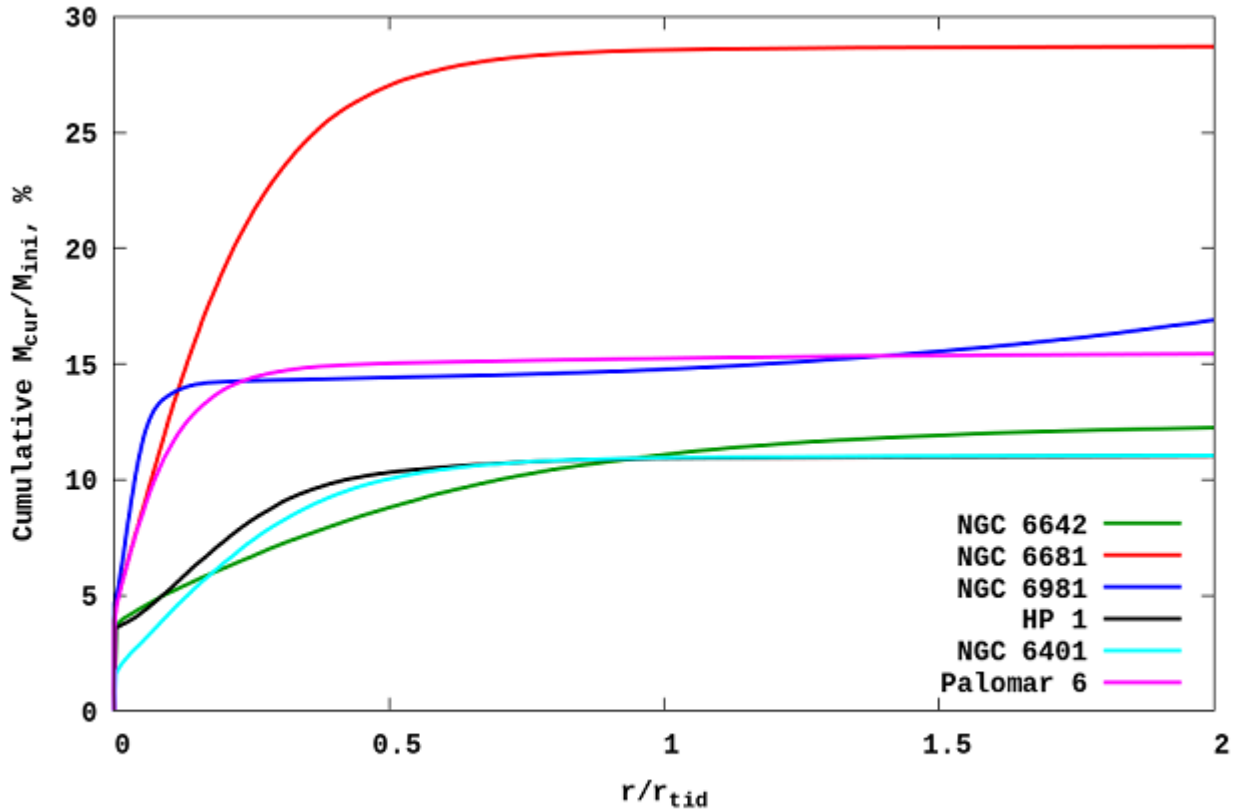

Fig. 4. Internal mass distribution of the GCs for today.

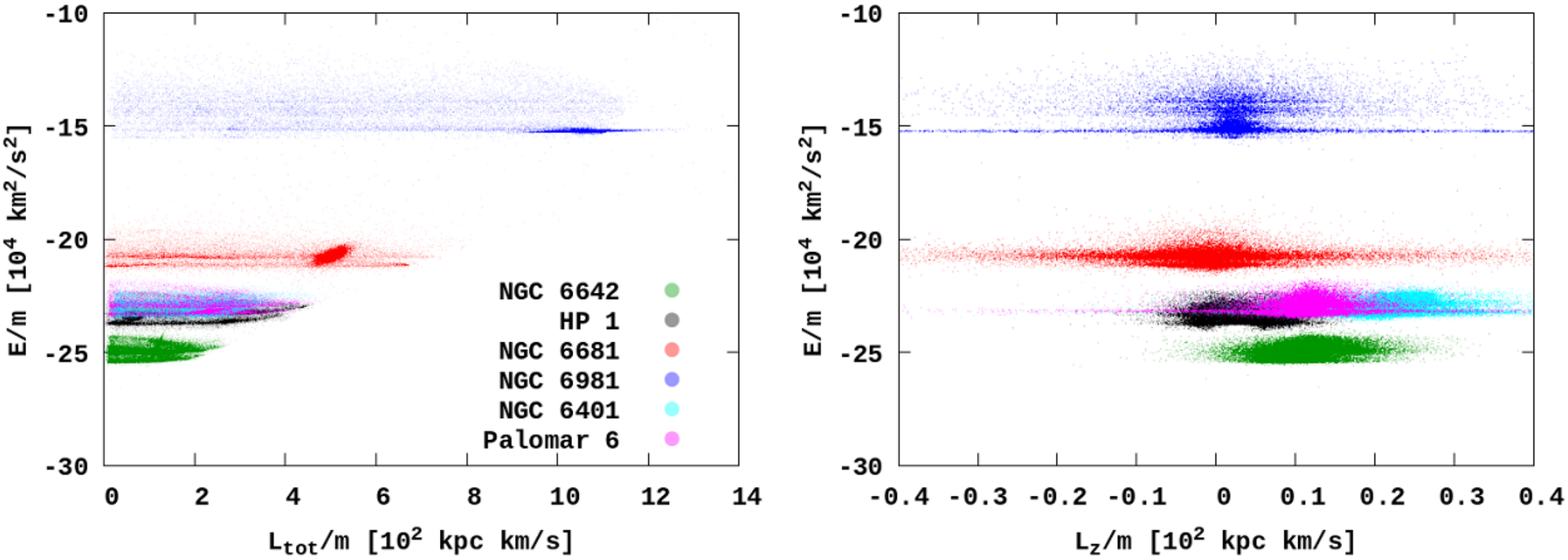

Fig. 10. Total energy (E/m) versus total angular momentum ($L_{\rm tot}/m$) and total energy versus z-th component of the angular momentum ($L_{\rm z}/m$) for GCs for today.

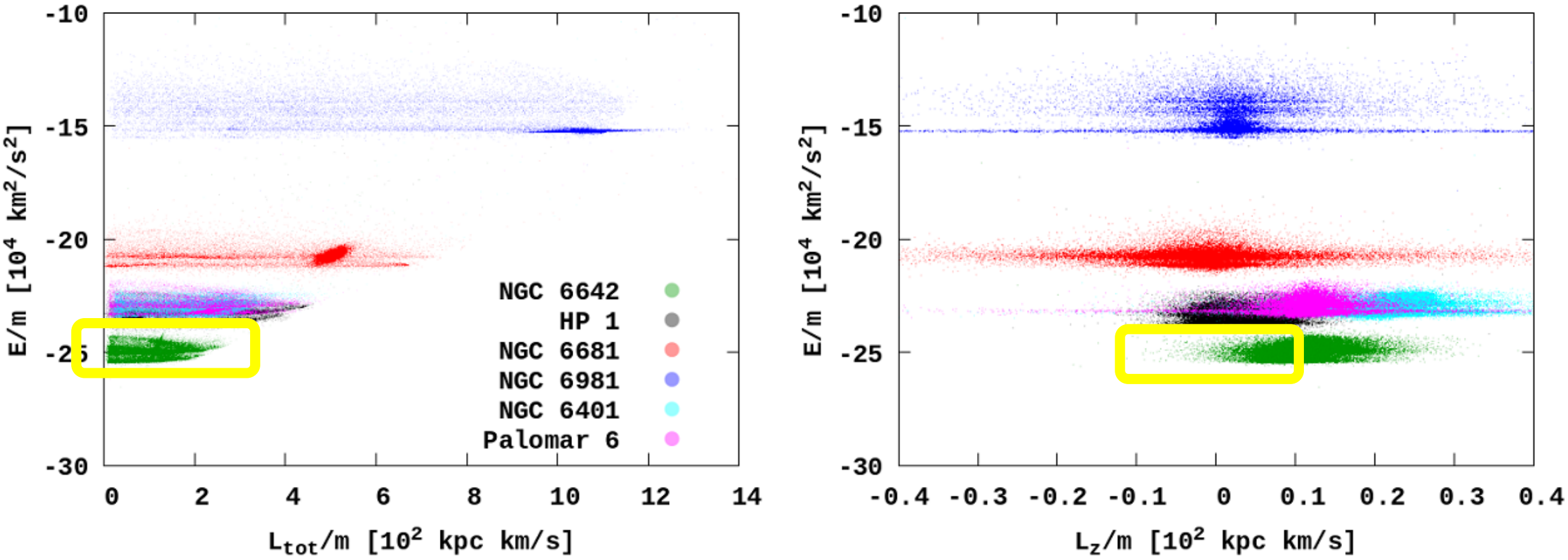

Fig. 10. Total energy (E/m) versus total angular momentum ($L_{\rm tot}/m$) and total energy versus z-th component of the angular momentum ($L_{\rm z}/m$) for GCs for today.

$$E^{*}_{\text{bound}} = -(M_{\text{NSC}} + m_{*})/R_{*} + V_{\text{red}} \cdot 0.5 \cdot V^{2}_{*},$$

Table 5. Total amount of the bound particles with the NSC and their masses with different velocity redaction during 8 billion years evolution in units of 10^3.

Vel_{red}	NGC 6642			NGC 6401			NGC 6681			HP 1		
	Tot.	Unq. / in %	$M_\odot$	Tot.	Unq. / in %	$M_\odot$	Tot.	Unq. / in %	$M_\odot$	Tot.	Unq. / in %	$M_\odot$
$V_{red=1.00}$	9.8	2.6 / 0.1	0.1	0.2	0.1 / 0.01	0.01	0	0	0	0	0	0
$V_{red=0.80}$	22	8 / 0.3	0.4	1.2	0.1 / 0.01	0.01	0	0	0	0	0	0
$V_{red=0.75}$	72	29 / 1.1	1.2	1.7	0.1 / 0.01	0.01	0	0	0	0	0	0
$V_{red=0.60}$	4 550	1 066 / 41	40.7	2.6	0.1 / 0.01	0.01	0	0	0	0	0	0
$V_{red=0.50}$	14 534	1 984 / 76	73.5	3.9	0.2 / 0.7	0.03	0	0	0	0	0	0
$V_{red=0.40}$	–	–	–	20	1.4 / 0.6	0.7	0	0	0	0	0	0
$V_{red=0.35}$	–	–	–	–	–	–	0	0	0	2 760	813 / 35	28.5
$V_{red=0.30}$	–	–	–	–	–	–	0.37	0.17 / 0.01	0.01	5 127	1 504 / 66	56.5
$V_{red=0.25}$	–	–	–	–	–	–	6.73	4.7 / 0.2	0.02	5 128	1 518 / 67	56.6
$V_{red=0.20}$	–	–	–	–	–	–	5 820	199 / 88	7.1	–	–	–

Notes. – indicates, that no calculations were carried out for these V_{red}.

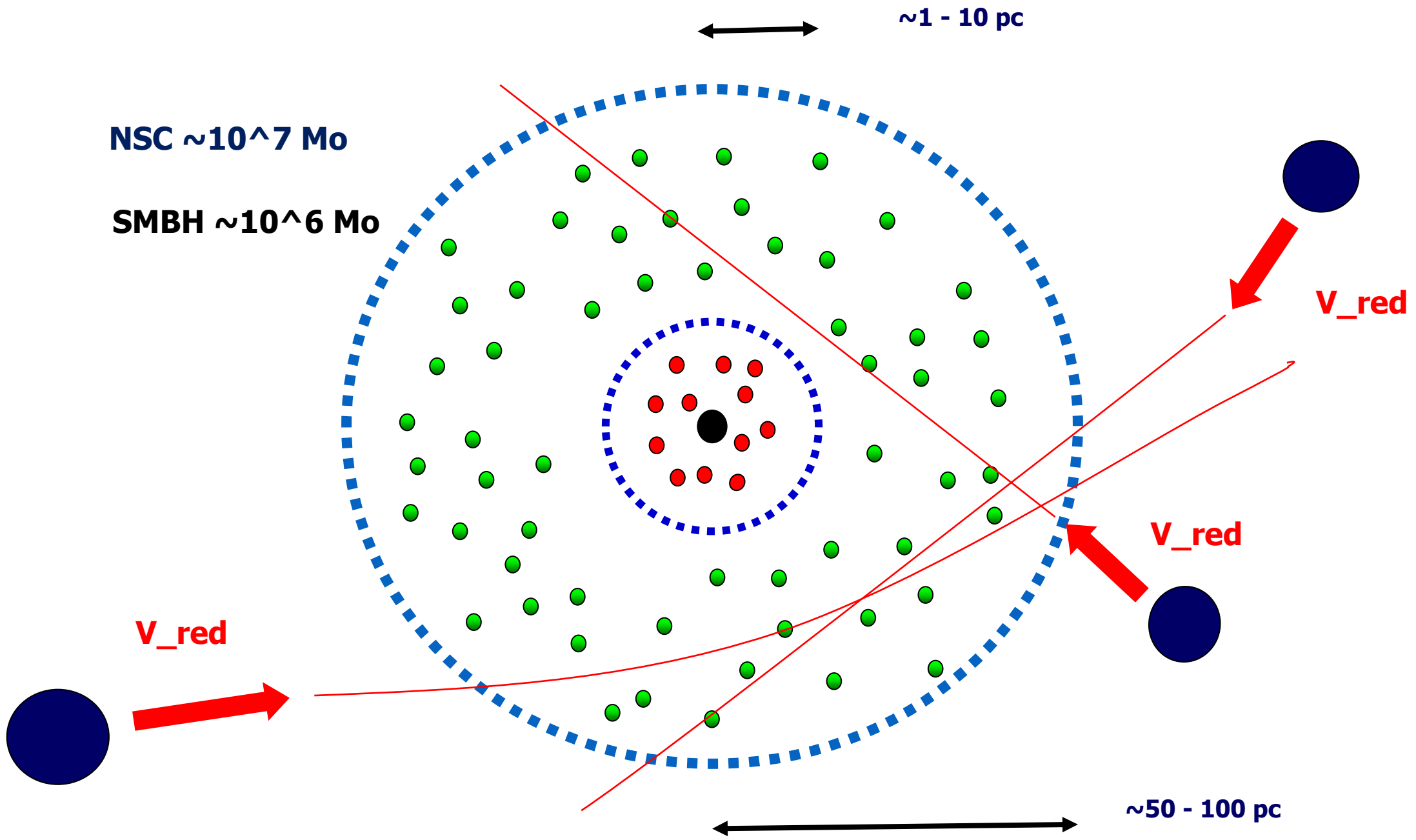
~1 - 10 pc
NSC ~10^7 Mo
SMBH ~10^6 Mo
V_red
V_red
V_red
~50 - 100 pc

Table 4. Total amount of NSs, BHs and BH systems formed in GCs.

GC	NS	BH	$N_{\text{sub-sys,BH}}$	$M_{\text{sub-sys,BH}}$, $M_\odot$
NGC 6401	12 480	3 570	1340	1.99×10^4
Palomar 6	13 540	3 020	1870	3.99×10^4
NGC 6681	15 910	3 970	2610	5.61×10^4
NGC 6642	17 730	4 440	2740	5.82×10^4
NGC 6981	11 710	2 990	1720	3.66×10^4
HP 1	15 140	3 890	2260	4.76×10^4

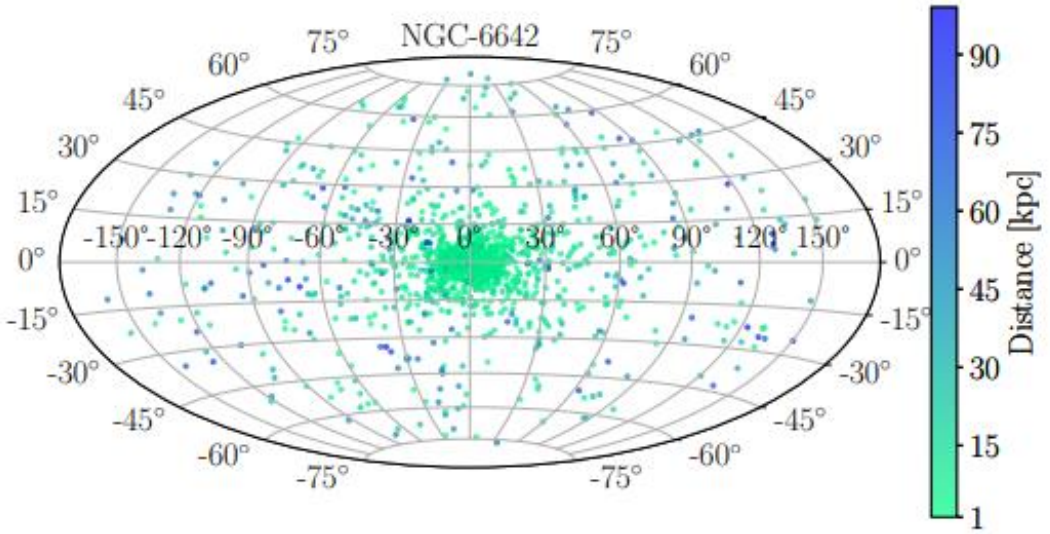

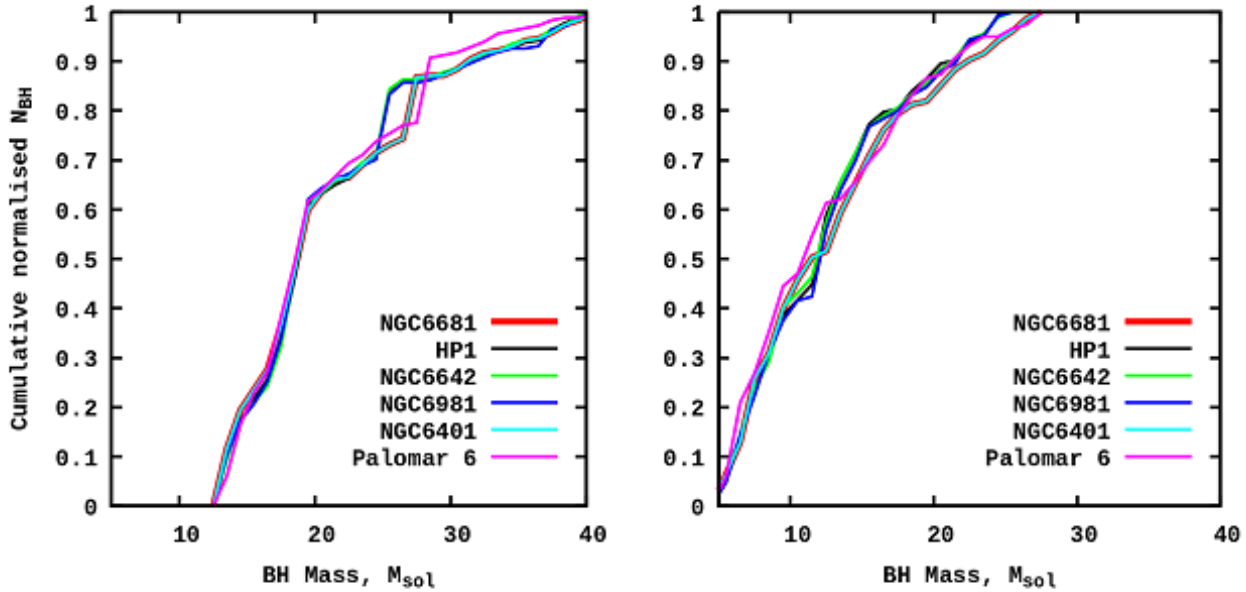

Fig. 7. Statistics of the natal kick dependency from the BH remnant final masses. For $V_{\text{kick}} = 0$ km s^{-1} – *left panel*, for $V_{\text{kick}} > 0$ km s^{-1} – *right panel*.

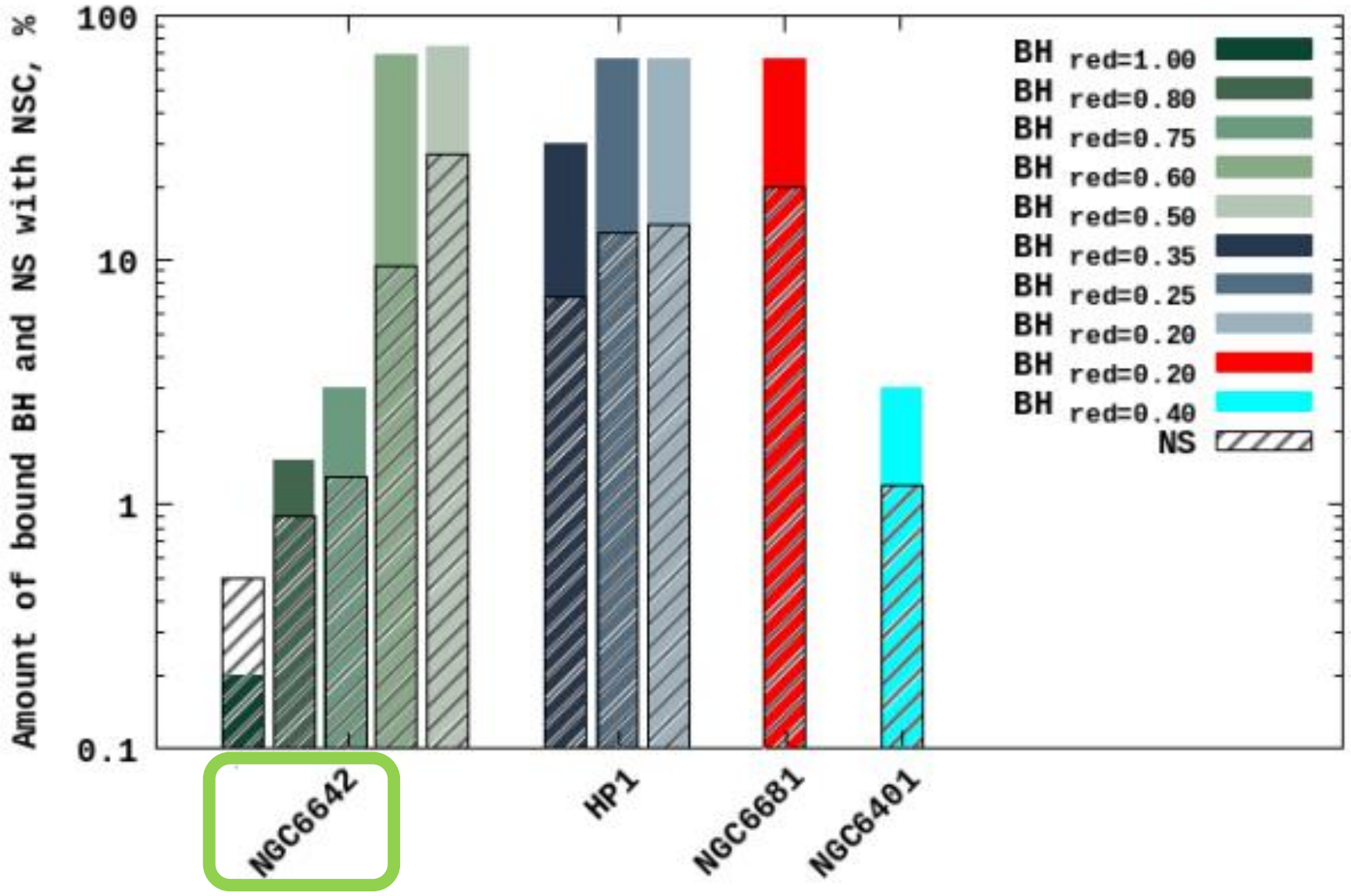

Fig. 16. Amount of compact stellar remnants bound with the NSC for NGC 6642, NGC 6401, HP 1 and NGC 6681.

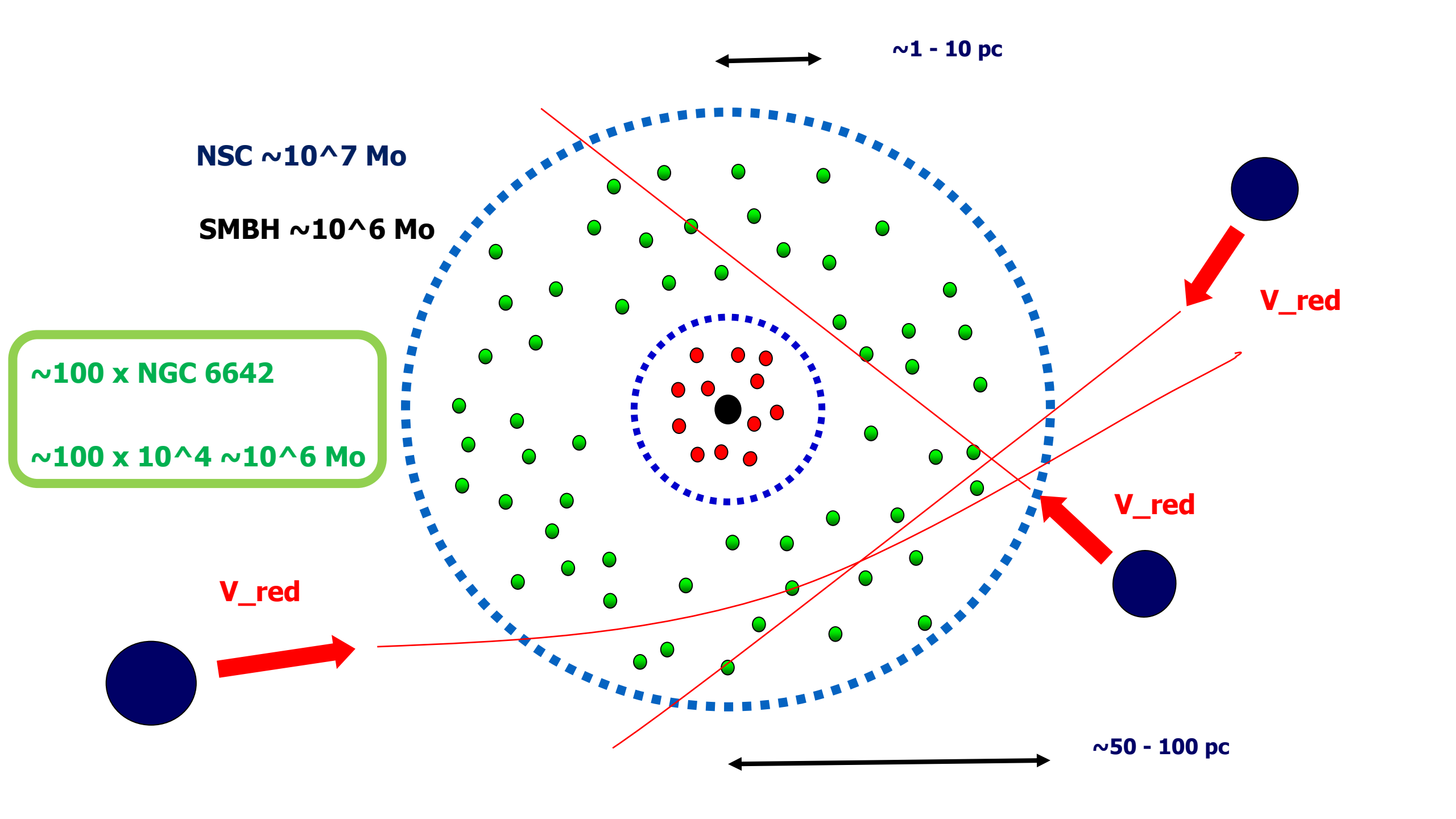
~1 - 10 pc
NSC ~10^7 Mo
SMBH ~10^6 Mo
~100 x NGC 6642
~100 x 10^4 ~10^6 Mo
V_red
V_red
V_red
~50 - 100 pc

Thank you for your attention...

☺